Evaluating an accelerated forcing approach for improving computational efficiency in coupled ice sheet-ocean modelling

Qin Zhou[1], Chen Zhao[2], Rupert Gladstone[3], Tore Hattermann[4,5], David Gwyther[6], and Benjamin Galton-Fenzi[2,7,8]

[1]Akvaplan-niva AS, Tromsø, Norway
[2]Australian Antarctic Program Partnership, Institute for Marine and Antarctic Studies, University of Tasmania, Hobart, Australia
[3]Arctic Centre, University of Lapland, Rovaniemi, Finland
[4]Norwegian Polar Institute, Tromsø Norway
[5]Energy and Climate Group, Department of Physics and Technology, The Arctic University - University of Tromsø, Norway
[6]Coastal and Regional Oceanography Lab, School of Biological, Earth and Environmental Sciences, UNSW Sydney, Sydney, NSW, Australia
[7]Australian Antarctic Division, Kingston, Australia
[8]The Australian Centre for Excellence in Antarctic Science, University of Tasmania, Hobart, Australia

Correspondence: Qin Zhou (qin@akvaplan.niva.no)

Abstract.

Coupled ice sheet-ocean models are increasingly being developed and applied to important questions pertaining to processes at the Greenland and Antarctic Ice Sheet margins, which play a pivotal role in ice sheet stability and sea level rise projections. One of the challenges of such coupled modelling activities is the timescale discrepancy between ice and ocean dynamics. This discrepancy, combined with the high computational cost of ocean models due to their finer temporal resolution, limits the time frame that can be modeled. In this study, we introduce an "accelerated forcing" approach to address the timescale discrepancy and thus improve computational efficiency in a framework designed to couple evolving ice geometry to ice shelf cavity circulation. This approach is based on the assumption that the ocean adjusts faster to imposed changes than the ice sheet, ~~with the ocean~~ so the ocean can be viewed as being in a ~~slowly varying~~ quasi-steady state that varies slowly over timescales of ice geometry change. By assuming that the ~~ocean-induced ice draft change~~ mean basal melt rate during one coupling interval can be reflected by a quasi-steady state ~~change~~ melt rate during a shortened coupling interval (equal to the regular coupling interval divided by a constant factor), we can reduce the ocean model simulation duration. We first demonstrate that the mean cavity residence time, derived from stand-alone ocean simulations, can guide the selection of suitable scenarios for this approach. We then evaluate the accelerated forcing approach by comparing basal melting response under the accelerated forcing with that under the regular forcing based on idealized coupled ice sheet-ocean experiments. Our results suggest that: the accelerated approach can yield comparable melting responses to those under the regular forcing when the model is subjected to steady far-field ocean conditions or time-varying conditions with timescales much shorter than the cavity residence time. However, it ~~is not~~ may not be suitable when the timescale of the accelerated ocean conditions is not significantly different from the cavity residence time. When ~~used carefully~~appropriately applied, the accelerated approach can be a useful tool in coupled ice sheet-ocean modelling.

1 Introduction

The Antarctic Ice Sheet represents the largest source of uncertainty in projections of sea level rise, with its contribution estimated to vary from -5 to 43 cm of sea level equivalent by 2100 under high carbon emission scenarios (Seroussi et al., 2020) emission scenarios (Seroussi et al., 2020, 2023). This uncertainty partly stems from the absence of ice sheet-ocean interactions in current sea level rise projections, which are based on stand-alone ice sheet models (Edwards et al., 2021; Seroussi et al., 2020). The interplay between the ice sheet and the ocean around Antarctica is a tightly coupled process and cannot be overlooked. Ocean-driven basal melting of floating ice shelves, influenced by ocean currents and ice draft geometry, can trigger a non-linear response impacting ice-shelf buttressing, grounded ice velocity, grounding line movements, and ice sheet instabilities (Gladstone et al., 2012; Favier et al., 2014). Conversely, glacial meltwater from the ice shelves affects water mass transformation, sea ice formation and melting, alongside regional and global ocean circulation (Foldvik et al., 2004; Jourdain et al., 2017; Li et al., 2023), while subglacial drainage injection into ice shelf cavities drives strong regional local melt increases (Nakayama et al., 2021; Gwyther et al., 2023) and impacts to sea ice formation (Goldberg et al., 2023). Moreover, stand-alone ice sheet models lack physically sound methods to compute basal melt rates under newly ungrounded ice (Jourdain et al., 2020). Therefore, coupled ice sheet-ocean models are essential for capturing the complexity of ice sheet-ocean interactions and thus improve sea level rise projections.

Driven by these needs, recent years have witnessed significant developments in coupled ice sheet-ocean modelling. Some studies follow the guidelines of the 1st Marine Ice Sheet-Ocean Model Intercomparison Project (MISOMIP1) on idealized domains (Asay-Davis et al., 2016; Favier et al., 2019; Zhao et al., 2022)(Asay-Davis et al., 2016; Favier et al., 2019; Zhao et al., 2022) , while others are based on realistic, regionally-scaled domains like the Totten Glacier Area (Pelle et al., 2021; Van Achter et al., 2023) (Pelle et al., 2021; Van Achter et al., 2023; McCormack et al., 2021), the Thwaites Glacier (Seroussi et al., 2017), the Filchner-Ronne Ice Shelf (Timmermann and Goeller, 2017; Naughten et al., 2021). More recently, coupled ice sheet-ocean model configurations on the circumpolar scale or beyond, with cavities explicitly resolved, have begun to emerge (Smith et al., 2021; Pelletier et al., 2022 , primarily in testing phases or for sensitivity studies (Muntjewerf et al., 2021). Applying (Smith et al., 2021; Pelletier et al., 2022; Siahaan . However, applying the circumpolar coupled ice-ocean models to long-term simulations is heavily constrained by the timescale discrepancy between ice and ocean dynamics. The ice sheet timescale ranges from decades to millennia, while the ocean timescale spans from hours to decades. As a result, the typical timestep sizes are smaller for ocean models (seconds to minutes) compared to those for ice sheet models (days to months), making the ocean model more computationally demanding to run. These limitations prevent the coupled models from running a longer-term and larger ensemble of simulations, both of which are important for sea level rise projections.

This challenge of timescale discrepancies is not unique to coupled ice sheet-ocean modelling. A number of different climate-related disciplines utilising coupled modelling have encountered these issues of optimising performance of a model system where individual components have varying response timescales, including atmosphere-ocean modelling (Sausen and Voss, 1996; Vo and paleo-climate modelling incorporating ice sheets (Roberts et al., 2014; Lofverstrom et al., 2020). Approaches have included "periodic synchronous coupling", where the outputs of the faster component are averaged over a short period of synchronous coupling and are then used to force the slower component(s) over a longer uncoupled period, and "asynchronous coupling", where the faster model is run for a shorter period during each coupling interval. In this context "synchronous coupling" simply means that the elapsed modelled time, measured at the time of any exchange of coupled variables, is the same for each component. There is a broader definition that has been recently used in the ice sheet - ocean community (Goldberg et al., 2018; Gladstone et , where "synchronous coupling" has been taken to mean that both fast and slow components update the coupling variables every fast timestep. Coupling synchronicity is especially important in the regional marine ice sheet - ocean modelling community where ice shelf cavity circulation is fully resolved by the ocean model but where the coupling region itself (the underside of the ice shelf) evolves with time.

In this study, we ~~introduce~~ extend the concept of asynchronous coupling by introducing an approach of "time compression" or "accelerated forcing" to address the challenge of timescale discrepancy between the ocean and ice-sheet models. With this approach, the temporal scale of the ocean model is adjusted to be α times faster than the real-time temporal scale. α is referred to as the acceleration factor throughout the text. This approach shares ~~a similar idea with~~ the approach of a morphological acceleration factor used by the sediment transport modelling community, which effectively extends the morphological simulation duration by multiplying the changes in bed sediments by a constant factor (Lesse et al., 2004; Li et al., 2018; Morgan et al., 2020).

In the context of coupled ice sheet-ocean modelling, the accelerated forcing approach is based on the assumption that the ocean adjusts faster to imposed changes than the ice sheet, with the ocean viewed as being in a slowly varying quasi-steady state over ~~timescales of ice geometry change~~over the timescales that matter for ice sheet geometry. Note that the quasi-steady state here refers to the spun-up phase where the ocean model maintains a consistent average response to external forcings~~over the timescales that matter for ice sheet geometry changes. Specifically, the oceanic effect on the~~ . Under this assumption, within the total ice draft change ~~Δz_d,~~ Δz_d, which includes contributions from ocean-driven change and ice-dynamics-driven change Δz_{di}, the ocean-driven draft change can be expressed as an integral of ~~ice draft change rate $\dot{z}_d(t)$~~ basal melt rate M over the coupling time interval T~~as~~ , as

$$\Delta z_d = \int^{T} (t) M \, dt, + \Delta z_{di}. \tag{1}$$

~~can be linearly decomposed into~~ The ocean-driven change can be further expressed as the time integral of a ~~slowly varying~~ quasi-steady-state ~~change rate $\overline{\dot{z}_d(t)}$~~ mean melt rate $\overline{M}^T$ over the coupling interval ~~as~~ T, as

$$\Delta z_d \int^{T} M \, dt = \overline{M}^T \cdot T. \tag{2}$$

By assuming that the ~~ice draft change rate $\overline{\dot{z}_d(t)}$~~ mean melt rate $\overline{M}^T$ during the coupling interval T can be ~~reflected~~ approximated by a quasi-steady-state ~~change rate $\overline{\dot{z}_d(t/\alpha)}$~~ melt rate $\overline{M}^{T/\alpha}$ during a shortened coupling interval of T/α, the ocean model simulation duration can be reduced from T to T/α, hereby accelerating the timescale of the ocean model by a factor of α. Note that the superscripts T and T/α denote the coupling intervals, not the exponents or powers of a number. In addition, to maintain the model's integrity under the accelerated approach, the timescales of the ocean model's boundary conditions should be also accelerated ~~, specifically by dividing them by a factor of α,~~ accordingly to accommodate the timescale change from T to T/α.

It is important to note that the above assumptions may not always hold true. However, our hypothesis proposes that this accelerated forcing approach remains valid under specific conditions - particularly when the quasi-steady state basal melting response is not sensitive to the boundary conditions that must be accordingly accelerated. This understanding provides a foundation upon which suitable scenarios for the approach can be determined. Specifically, it emphasizes the need to investigate how the basal melting in the ocean model responds to boundary conditions with varying timescales~~: the~~ . In a regional coupled ice sheet-ocean model system, the ocean model is subject to a range of boundary conditions: changes in ice draft, heat and meltwater fluxes at the ice sheet-ocean interface, momentum, freshwater, and radiation fluxes at the atmosphere-ocean interface, and far-field ocean conditions~~outside of the ice shelf cavity~~ . In this study, we only focus on the far-field ocean conditions and the ice draft change at the ice sheet-ocean interface, as these two factors predominantly control the cavity circulation and, thus, the basal melting response.

The far-field ocean conditions influencing ice sheet-ocean interactions around Antarctica range from seasonal, sub-decadal and decadal fluctuations ~~(Dutrieux et al., 2014; Jenkins, 2016)~~ (Dutrieux et al., 2014; Jenkins, 2016; Paolo et al., 2018; Jenkins et al., 2018 , to longer, century-scale shifts associated with climate warming (Hellmer et al., 2012; Naughten et al., 2021). Given such vast variability, the systematic testing of the feasibility of the accelerated forcing approach becomes inefficient. Nevertheless, Holland (2017) suggests that the melting to time-varying ocean forcing is dictated by the relative magnitude of two timescales, the forcing timescale and the mean cavity residence time that is the characteristic time taken for the barotropic circulation to flush the entire cavity~~(Holland, 2017)~~. The basal melting remains relatively stable when the cavity is subject to ocean conditions varying more rapidly than the cavity residence time, suggesting a scenario where the accelerated forcing approach might be applicable. However, the approach's applicability under ocean conditions, which vary slower than the cavity residence time, requires further experimental investigation. Following Holland (2017)'s study of exploring the melting response to time-varying ocean forcing, we will first use stand-alone ocean models with fixed ice cavities to identify the suitable scenarios for pragmatically applying the accelerated forcing approach.

The study is organized as follows: Section 2 briefly introduces the implementation of the accelerated forcing approach in the coupled ice sheet-ocean system. Section 3 explores the basal melting to ~~oscillating~~ time-varying far-field ocean conditions to determine suitable scenarios for the ~~accelerated~~ approach with stand-alone ocean experiments. Section 4 ~~evaluates the accelerated forcing approach for~~ assesses the approach across three scenarios with ~~coupled ice sheet-ocean experiments with the MISOMIP1 framework~~varied far-field ocean conditions using idealized coupled model setups. Lastly, Section 5 summarizes the findings and discusses the applicability and limitations of the approach.

2 Methodology and model description

2.1 The coupler: FISOC

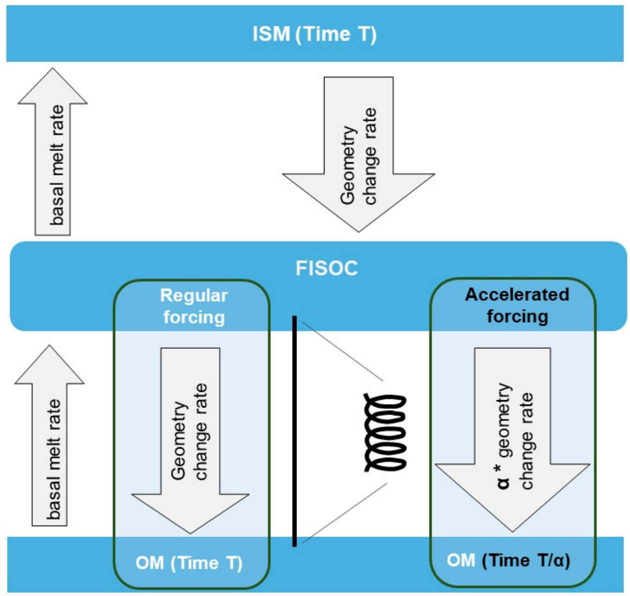

Figure 1. Data flow for the coupled ice sheet-ocean ~~coupled~~ model system using FISOC, ~~indicating~~ illustrating the ~~difference~~ differences between the regular forcing and ~~the~~ accelerated forcing ~~approach~~approaches. ISM and OM stand for ice sheet model and ocean model, respectively. With the regular forcing approach, geometry change rate and basal melt rate are exchanged at regular time intervals. With the accelerated forcing approach, the geometry change rate passed to the ocean model is adjusted by multiplying it by the acceleration factor (α).

The current study implements the accelerated forcing approach within the Framework For Ice Sheet–Ocean Coupling (FISOC). This flexible coupling framework, adopting the hierarchical modular structure of the Earth System Modelling Framework, allows exchange of data between ice sheet and ocean models at the underside of the ice shelves (Gladstone et al., 2021). Figure 1 illustrates the workflow of the coupled ice sheet-ocean model system, both with and without the accelerated forcing approach. In the absence of the accelerated forcing approach as ”regular forcing” within FISOC, the basal melt rates, calculated by the ocean model, are passed from the ocean model to the ice model, while geometry change rates, determined by the ice model, are passed from the ice model to the ocean model, as

$$\frac{dz_d}{dt}_{[O]} = \frac{dz_d}{dt}_{[I]}. \tag{3}$$

Here z_d is the ice draft, and subscripts in square brackets indicate the representation of the same property within either the ice [I] or ocean [O] component. This exchange occurs at a coupling interval of T. Conversely, under the ”accelerated forcing” approach with an acceleration factor α, the boundary conditions imposed by the ice sheet model on the ocean model must be adjusted accordingly. Specifically, the geometry change rates received by the ocean model are amplified by a factor of α, as

$$\frac{dz_d}{d(t/\alpha)}_{[O]} = \alpha \frac{dz_d}{dt}_{[O]} = \alpha \frac{dz_d}{dt}_{[I]}. \tag{4}$$

As the ocean model is run for a period of T/α each coupling interval instead of T, the total change in ice geometry experienced by the ocean model during one coupling interval is the same under the accelerated forcing as the regular forcing. But the computational efficiency has been increased α times. It is important to note that throughout the text, we distinguish between *model time*, which refers to the ocean model's actual simulation time (T/α for one coupling interval), and *represented time*, which signifies the real world time represented by the model, calculated as the model time multiplied by the acceleration factor (T for one coupling interval).

2.2 The ~~ice-sheet~~ ice sheet model, Elmer/Ice

~~For the ice model in the coupled simulations, we~~ We use Elmer/Ice, a finite-element, dynamic ice sheet model (Gagliardini et al., 2013)~~. Here, the~~ , as the ice model component in the coupled model system. The ice sheet model setup in this study is following Zhao et al. (2022). We use the Shallow Shelf Approximation (SSA*) solution, a variant of the L1L2 solution of Schoof (2010), ~~is used~~ to solve the shallow shelf approximation of the Stokes equations~~.The SSA* approximation~~ , which accounts for longitudinal and lateral stresses with an assumption of a simplified vertical shearing in the effective strain rate to represent fast-flowing ice streams and ice shelves. ~~The SSA* approximation was recently coupled with the ocean model ROMS using FISOC (Zhao et al., 2022), and the same configuration is used in this study. A constant~~ We apply a surface mass balance rate of 0.3 ~~$\mathrm{m\,yr^{-1}}$ is applied here.~~

~~We~~ $\mathrm{m\,yr^{-1}}$ and assume a constant ice temperature in the ice model and zero heat flux across the ice-ocean boundary. The ice front location does not vary with time and the ice mass loss due to calving disappears immediately without any freshwater flux into the ocean. ~~A~~ We also apply a non-linear Weertman-type sliding relationship (Eq. (21) in Gagliardini et al. (2013)) ~~was applied~~ for grounded ice, with a sliding parameter equal to 0.01 $\mathrm{MPa\,m^{\frac{1}{3}}\,a^{\frac{1}{3}}}$ and an exponent equal to $\frac{1}{3}$. The shelf regions are free slip.

2.3 The ocean models, FVCOM and ROMS

To increase the generality of our ~~evaluations~~ evaluation of the accelerated forcing approach, we conduct our main experiments using two different regional ocean models. The primary model is the Finite Volume Community Ocean Model (FVCOM) (Chen et al., 2003). While FVCOM is noted for its unstructured grid allowing geometric flexibility to resolve small-scale ice sheet-ocean interaction processes (Zhou and Hattermann, 2020), it is chosen here due to the authors' expertise with the model and its potential applications in future work. We also conduct selected experiments with the Regional ~~Oceanic modelling~~ Ocean Model System (ROMS~~) (Shchepetkin and McWilliams, 2005). ROMS~~ , (Shchepetkin and McWilliams, 2005), which employs a structured Arakawa C-grid and has been widely used for resolving ice shelf cavities around Antarctica (Dinniman et al., 2007; Naughten et al., 2018; Galton-Fenzi et al., 2012; Richter et al., 2022). In addition to different ~~grids~~grid structures, the two

Table 1. Characteristics of the FVCOM and ROMS configurations used in this study.

	FVCOM	ROMS
Horizontal grid	unstructured triangle grid	structured C-grid
Horizontal discretization	finite volumes	finite differences
Horizontal mixing scheme	Eddy closure parameterization	Laplacian mixing scheme
Vertical mixing scheme	Mellor and Yamada level 2.5	K-Profile Parameterization

models differ in many aspects including numerical discretization, advection schemes, and mixing scheme parameterizations. Table 1 outlines some key differences in model characteristics between FVCOM and ROMS. However, it is worth noting that both models employ terrain-following vertical coordinates and share a number of similarities in resolving ice shelf cavities, including:

- Ice shelf-ocean thermodynamics are parameterized by the three-equation formulation following Jenkins et al. (2010). Specifically, in both models, values of $Cd = 0.0025$, $\Gamma_{\mathrm{T}} = 0.05$, and $\Gamma_{\mathrm{S}} = 0.0014$ are used for the drag coefficient and the turbulent heat and salt exchange coefficients, respectively.
- Both ocean models account for the thermodynamic effect of basal melting by imposing virtual heat and salt fluxes within a fixed geometry at each ocean model time step, to mimic the effects of basal melting, rather than employing an explicit volume flux at the ice-ocean interface.
- Ice shelf mechanical pressure is given by the density at the first layer of the model minus an assumed linear dependence of the density with depth, following Dinniman et al. (2007).
- In coupled model setups, the grounding line movement is realized by the wet and dry scheme, allowing a passive water column under the grounded ice and an active water column under floating ice or in the open ocean. Note that the passive layer is very thin when dry and gets expanded when wet.

3 Stand-alone ocean experiments

3.1 Experiment design

To increase the generality of our investigations of melting response to ~~ocean forcing with varying timescales~~time-varying far-field ocean conditions, we employ two model domains differing in ice cavity geometry that is fixed in time for our stand-alone ocean experiments. The first, as illustrated in Figure 2, is the Ice Shelf ~~-~~– Ocean Model Intercomparison Project (ISOMIP+) domain (Asay-Davis et al., 2016). It features a rectangular box bounded by $320\ \mathrm{km} \leq \mathrm{x} \leq 800\ \mathrm{km}$ in the x direction and $0 \leq \mathrm{y} \leq 80\ \mathrm{km}$ in the y direction, with the ~~initial~~ grounding line position at $\mathrm{x} = 460\ \mathrm{km}$. The second domain

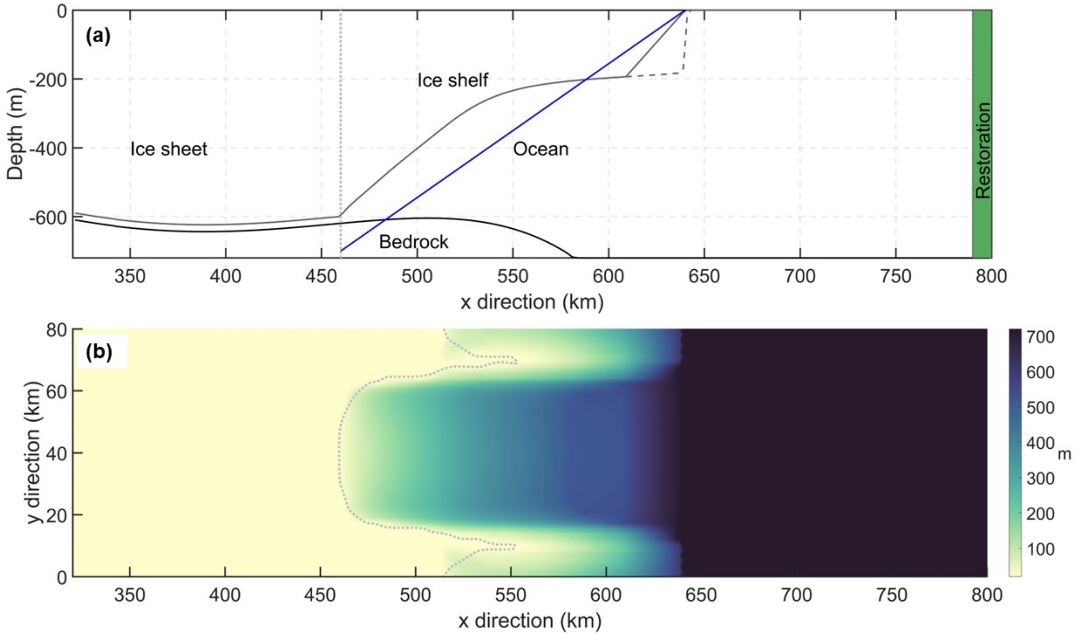

Figure 2. Panel (a) ~~Cross-sectional~~ shows a cross-sectional view along the center of the ISOMIP+ domain~~showing various~~ , highlighting key components: the bottom topography (black line), the initial grounding line position (light gray ~~straight~~ dashed line), and the ice shelf geometry used in ~~FVCOM~~ the FVCOM-ISOMIP+ simulations (dark grey line). Note that ~~ROMS~~ the ROMS-ISOMIP+ configuration uses the same ice shelf geometry except at the ice front (610 km $\leq x \leq$ 640 km), ~~and~~ where the ~~curry-color~~ grey dashed line denotes the ice front as ~~utilized~~ used in ~~ROMS~~ the ROMS-ISOMIP+ simulations. The ~~red~~ blue line indicates the ice shelf geometry used in ~~FVCOM simulations with~~ the ~~Wedge cavity~~FVCOM-Wedge simulations. The green shaded area marks the region of ~~far-field~~ ocean forcing restoration~~utilized by the ocean model~~. Panel (b) ~~Plain-view~~ display a plane view of the ISOMIP+ domain, with color shading indicating the water column thickness. The light grey dashed lines denote the initial boundary separating the wet cells (to the right) and the dry cells (to the left). This ISOMIP+ domain also serves as the domain for the ocean ~~components~~ component in the coupled ice sheet-ocean experiments.

features the same rectangular box but with a simplistic, wedge-shaped ice shelf in a flat-bottom ocean (Figure 2a), henceforth referred to as the "Wedge". The wedge domain is implemented only in FVCOM, resulting in three model configurations: FVCOM-ISOMIP+, FVCOM-Wedge, and ROMS-ISOMIP+.

All configurations have a horizontal resolution of 2 km. The only external forcing in the model is a restoring forcing of far-field ocean conditions within 10 km of the lateral boundary of the domain (790 km $\leq$ x $\leq$ 800 km), as indicated by the green area in Figure 2a. The initial ocean properties and far-field ocean conditions consist of horizontally homogeneous temperature and salinity profiles that vary linearly with water depth:

$$T = T_0 + (T_b - T_0)\frac{z}{D} \quad (5)$$

and

$$S = S_0 + (S_b - S_0)\frac{z}{D}, \quad (6)$$

where $D = 720$ m is the maximum water depth, and T_0, S_0 and T_b, S_b denote the surface and bottom values for temperature and salinity, respectively. Depending on the experiment, the temperature and salinity profiles used are either constant or oscillating over time. For constant profiles, as detailed in Table 2, we adopt the COLD and WARM profiles from Asay-Davis et al. (2016). These profiles represent typical ocean conditions near Antarctic ice shelves, with "COLD" and "WARM" referring to the conditions near cold and warm ice shelves, respectively. The MEAN profiles, derived by averaging the COLD and WARM profiles, qualitatively represent average ocean properties.

The oscillating profiles are conducted as repeating cosine waves, fluctuating between the COLD and WARM profiles with a period P as

$$T_P(t) = 0.5(T_W + T_C) - 0.5(T_W - T_C)cos(\frac{2\pi}{\mathrm{P}}t), \quad (7)$$

and

$$S_P(t) = 0.5(S_W + S_C) - 0.5(S_W - S_C)cos(\frac{2\pi}{\mathrm{P}}t). \quad (8)$$

Here T_P and S_P stand for the oscillating profiles for potential temperature and salinity, respectively. T_W and S_W are the linear ~~warm~~ WARM profiles for potential temperature and salinity, respectively, and T_C and S_C are the linear COLD profiles for potential temperature and salinity, respectively. When averaged over the period P, these oscillating profiles yield the MEAN profiles.

Table 3 summarizes the stand-alone ocean experiments. For each configuration, we conduct three constant forcing simulations and a number of oscillating forcing simulations with different periods. Specifically, oscillation periods for FVCOM-ISOMIP+ are 0.1, 0.2, 0.6, 1, 2, 6, 10, 20, and 30 years. Periods for FVCOM-Wedge are 0.1, 0.2, 1, 2, 10, and 20 years. Periods for ROMS-ISOMIP+ are 0.4, 4, 8, 20, and 36 years. While all the constant forcing simulations are initialized from the COLD ~~rest state~~rest-state cavity, the oscillating simulations are initialized from the spun-up state of the respective COLD forcing simulations. Each simulation was run until a quasi-equilibrium state was achieved, characterized as a constant state of mean melting for the constant forcing simulations and a repetitive state for the oscillating forcing simulations. Here the quasi-equilibrium state refers to the model's spun-up phase, in which the model's outputs are no longer influenced by the initial conditions but are instead determined by the external forcings. Unless stated otherwise, our analysis is based on results from a quasi-equilibrium state, which are time-averaged over the final year of model time for constant forcing simulations and over the last cycle for oscillating forcing simulations.

3.2 Melting response to oscillating ocean forcing

As we will explore the melting response to oscillating ocean forcing in comparison with the constant MEAN forcing, it is necessary first to examine the melting response from the simulations restored to the MEAN profiles. Throughout the text, all the

Table 2. Summary of parameters for the temperature and salinity profiles. Note that all salinities on the practical salinity scale (PSS-78).

Profiles	Surface temperature, T_0	Bottom temperature, T_b	Surface salinity, S_0	Bottom salinity, S_b
COLD	-1.9°C	-1.9°C	33.8	34.55
MEAN	-1.9°C	-0.45°C	33.8	34.625
WARM	-1.9°C	1°C	33.8	34.7

Table 3. Summary of stand-alone ocean experiments.

Experiment class	Simulation name	Initial state	Restoring forcing profiles
FVCOM-ISOMIP+	FI_C2C	at rest, COLD	COLD
	FI_C2M	at rest, COLD	MEAN
	FI_C2W	at rest, COLD	WARM
	FI_P	FI_C2C spun-up state	oscillating, period P
FVCOM-Wedge	FW_C2C	at rest, COLD	COLD
	FW_C2M	at rest, COLD	MEAN
	FW_C2W	at rest, COLD	WARM
	FW_P	FW_C2C spun-up state	oscillating, period P
ROMS-ISOMIP+	RI_C2C	at rest, COLD	COLD
	RI_C2M	at rest, COLD	MEAN
	RI_C2W	at rest, COLD	WARM
	RI_P	RI_C2C spun-up state	oscillating, period P

measures derived from these MEAN forcing simulations are referred to as mean-state measures. Despite their different cavity geometries, the two ~~FVCOM~~ FVCOM-based MEAN forcing simulations ~~(FI_C2M and FW_C2M)~~ exhibit similar barotropic circulation patterns ~~, as illustrated in~~ (Figure 3a and c). Both simulations display a single clockwise gyre in the open ocean. Within the ice cavity, the circulation primarily exhibits a geostrophically controlled flow, featuring an inflow of boundary waters across the ice front and along the lower flank and an outflow along the upper flank. Consequently, in both ~~FVCOM~~ FVCOM-based simulations, intense melting is observed near the deepest part of the lower flank, while significant freezing occurs along the upper flank (Figure 3b and d). However, the strength of the circulation and the associated melting-freezing process varies with the different ice cavity geometries. Notably, The simulation with the ISOMIP+ cavity (FI_C2M; Figure 3a) exhibits much weaker circulation compared to that with the wedge cavity (FW_C2M; Figure 3c), highlighting the effect of cavity geometry on the circulation and, consequently, on melting patterns.

Table 4. Melting diagnostics for simulations restored to the MEAN profiles across different model configurations.

Simulation name	Cavity volume (m^3)	Cavity-averaged barotropic streamfunction (Sv)	Cavity-averaged melt rate (myr^{-1})	Mean cavity residence time (yr)
FI_C2M	3.9×10^{12}	0.03	1.87	~ 4
FW_C2M	4.6×10^{12}	0.07	2.7	~ 2
RI_C2M	3.75×10^{12}	0.018	0.97	~ 7

In contrast, despite using the same ISOMIP+ cavity and being restored to the same MEAN profiles, the ROMS simulation (RI_C2M) ROMS-based MEAN forcing simulation exhibits distinct barotropic circulation patterns (Figure 3e) compared to its FVCOM counterpart (FI_C2M;Figure 3a). Specifically, RI_C2M it features three gyres in the open ocean and an inflow across the lower part of the ice front ($y = 0 - 20$ km), along with an anti-clockwise gyre near the ice front in the cavity. Additionally, basal melting in RI_C2M the ROMS-based simulation (Figure 3f) is generally weaker than that in FI_C2M the FVCOM-based simulation (Figure 3b). It is important to note that our focus here is to understand the melting response within each model configuration to oscillating ocean forcing, rather than directly comparing the two models. The observed differences between the ROMS and FVCOM MEAN forcing ROMS-based and the FVCOM-based ISOMIP+ simulations may reflect a combination of differences in model numerics (Table 1) and artifacts associated with the pressure gradient error (Zhou and Hattermann, 2020). The ISOMIP+ cavity ice front in the FVCOM FVCOM-based simulation was smoothed to mitigate the pressure gradient error, unlike in the ROMS ROMS-based simulation, likely leading to a smaller pressure gradient error.

Table 4 presents cavity-averaged melt rates alongside with the mean-state cavity residence time (MCRT) from these three MEAN forcing simulations.The MCRT, computed by dividing the cavity volume by the cavity-averaged barotropic streamfunctions, represents the time required for all the cavity waters to be flushed with the MEAN forcing waters to fully affect the basal melting (Holland, 2017). Next we will use the MCRT as a key timescale for investigating the response of basal melting to oscillating ocean restoring conditions.

Figure 4 displays the time series of domain-averaged temperatures and cavity-averaged melt rates from selected simulations for each of the three model configurations: three constant forcing simulations (COLD, MEAN, and WARM) and three oscillating simulations with periods that are either shorter than 0.1 times the MCRT, close to or within 2 times the MCRT, or significantly longer than 5 times the MCRT. Across the three model configurations, the WARM forcing simulation displays the highest temperatures and, consequently, the highest melt rates. Notably, Although although the mean-state temperature is intermediate between the WARM and COLD simulations, the corresponding mean-state melt rate stays more closely with the COLD simulation, rather than evenly between the two. This suggests a non-linear, possibly quadratic relation between ocean temperatures and melt rates (Holland et al., 2008b)(Holland et al., 2008b; Jenkins et al., 2018).

In all the oscillating simulations, both the temperature curve forcing simulations, time series of the temperatures and the melt rate curve rates exhibit oscillation patterns that reflect the periods of the respective ocean forcing. MoreoverAdditionally,

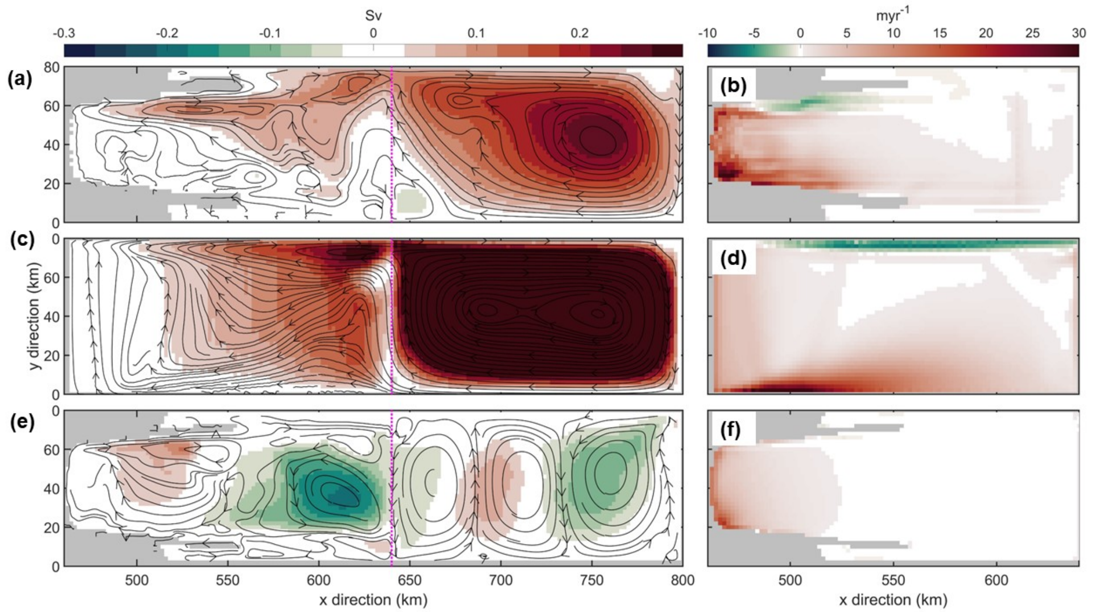

Figure 3. ~~The left column shows plan~~ Panels (a), (c), and (e) show plane views of the quasi-steady state barotropic streamfunction from the simulations restored to the MEAN profiles for the FVCOM-ISMOP+ (FI_C2M~~(a)~~), FVCOM-Wedge (FW_C2M~~(c)~~), and ROMS-ISOMIP+ (RI_C2M~~(e)~~) configurations, ~~with~~ respectively. The black lines and arrows ~~indicating~~ indicate the barotropic flow~~and~~, while the ~~yellow~~ magenta dashed line ~~marking~~ mark the ice front~~location~~. ~~The right column presents plan views~~ Panels (b), (d), and (f) display spatial distribution of ~~the basal~~ melt rates from the ~~same simulations:~~ simuations FI_C2M~~(b)~~, FW_C2M~~(d)~~, and RI_C2M~~(f)~~, respectively.

the melt rate ~~curves~~time series, particularly in the longer-period simulations (orange lines in Figure 4d,e,f), exhibit a distinct asymmetrical shape ~~. Specifically, this asymmetry is~~ characterized by broader low melt troughs ~~, representing phases when the cavity is filled with COLD water, in contrast to~~ and narrower high melt peaks~~, indicative of phases with WARM water in the cavity~~. The asymmetry is related to the internal feedback between cavity circulation and boundary forcing (Holland, 2017). During a forcing cycle where the far-field ocean conditions vary from WARM to COLD and back to WARM, when the cavity is filled with WARM water, the enhanced melting leads to faster cavity circulation, facilitating quicker flushing of COLD water and rapid cooling of the cavity. Conversely, in a COLD cavity state, the circulation slows, extending the time taken to flush WARM water into the cavity, hence resulting in a slower warming phase. ~~This~~ The asymmetry is also visible in the melt rate time series from the simulations with forcing periods close to the ~~CMRT~~ MCRT (blue lines in Figure 4d,e,f).

~~In Figure 4d, e, and f, the melt rate curves from simulations subjected to oscillating forcing exhibit~~ Furthermore, the temporal melting responses from the oscillating forcing simulations share common features across ~~different model configurations~~ the three model configurations (Figure 4d, e, and f): i) for periods significantly shorter than the MCRT, indicated by green lines, melt rates are slightly above their respective mean-state values; ii) for periods close to the MCRT, shown by cyan lines, ~~the majority of melt rates fall beneath~~ most of the melt rates within each cycle fall below the mean-state values, suggesting reduced melting in these simulations; iii) for periods substantially longer than the MCRT, as depicted by orange lines, ~~peak or trough melt rates reach or are near those seen in~~ the maximum (minimum) melt rates are close to or equal to those from the respective WARM ~~or COLD~~(COLD) forcing simulations, ~~suggesting that melting is nearly in equilibrium with the periodic forcing at all times. Additionally, the majority of melt rates lie~~ with a greater portion of the melt rates above the mean-state ~~values~~value in each cycle.

These features are also evident in the spatial distributions of melt rate deviations from the selected oscillating forcing simulations, relative to their respective mean-state melt rates (Figure 5). For periods significantly shorter than the MCRT (~~FI_0.2yr, FW_0.1yr and RI_0.4yr; top row~~ the top row panels in Figure 5), enhanced melting is mainly observed in the inner part of the cavity, with the cavity-averaged melt rates increasing by 10%, 5% and 14%. For periods close to the MCRT (~~FI_6yr, FW_2yr, and RI_10yr), the spatial distribution shows~~ the middle row panels in Figure 5), a significant reduction in melting appears at locations of strong mean-state melting, ~~as compared with the mean-state melting pattern illustrated in Figure 3b, c, and e. The~~ with the cavity-averaged melt rates decrease by 31%, 29% and 29%. For periods substantially longer than the MCRT (~~FI_30yr, FW_20yr and RI_36yr; bottom row~~ the bottom row panels in Figure 5), there is a general increase in melting, particularly in the inner part of the cavity in the two ~~FVCOM simulations (FI_30yr and FW_20yr~~FVCOM-based simulations (Figure 5g,h), with the cavity-averaged melt rates rising by 29%, 12% and 13%.

Figure 6 provides a qualitative summary of melting response to oscillating forcing across all the simulations in three model configurations, by depicting the relationship between normalized melt rate and normalized timescale. The normalized melt rate is computed by dividing the cavity-averaged melt rate in each oscillating forcing simulation by the corresponding mean-state cavity-averaged melt rate. Similarly, the normalized timescale is the ratio of the oscillating period to the respective MCRT. As we use Log2(Normalized timescale) for the x-axis in the figure, a value of 0 indicates a forcing oscillation period close to the MCRT, a value of -2 indicates a forcing period of 0.25 times the MCRT, while a value of 2 indicates a forcing period of 4 times the MCRT.

Figure 6 not only reinforces the three distinct melting regimes observed in the time series and spatial distribution figures but also provides ~~two additional key insights crucial for determining the applicability of the~~ additional insights for predetermining suitable scenarios for the accelerated forcing approach. ~~Firstly, when oscillation periods~~ First, the normalized melt rates reach their minimum across all three model configurations when the oscillation periods approximate the MCRTs (Log2(Normalized timescale) $\approx$ 0). In this regime, melt-induced circulation begins to increase with the warm phase of the oscillation just as the forcing shifts back to the cold phase, which rapidly cools the cavity. The return to the warm phase is slower due to diminished melt-induced circulation in the cold phase, resulting in a cavity temperature closer to the COLD profiles, thereby minimizing melting. This suggests that with any adjustments in the timescale when the oscillation period approximates the MCRT, the melting response is likely to deviate significantly from the mean melting response. Secondly, when oscillation periods are shorter than the MCRT (Log2(Normalized timescale) ~~$<$~~$<$ 0), the melting rates tend to stabilize, as indicated by normalized melt rates clustering between 0.9 and 1.1. ~~This is because multiple COLD and WARM waters coexist within the cavity in this regime , effectively canceling each other in the spatial mean,~~ In this regime where the ocean conditions oscillate rapidly, the ocean temperature doesn't have time to adjust to that of the WARM or COLD profiles. This results in the water

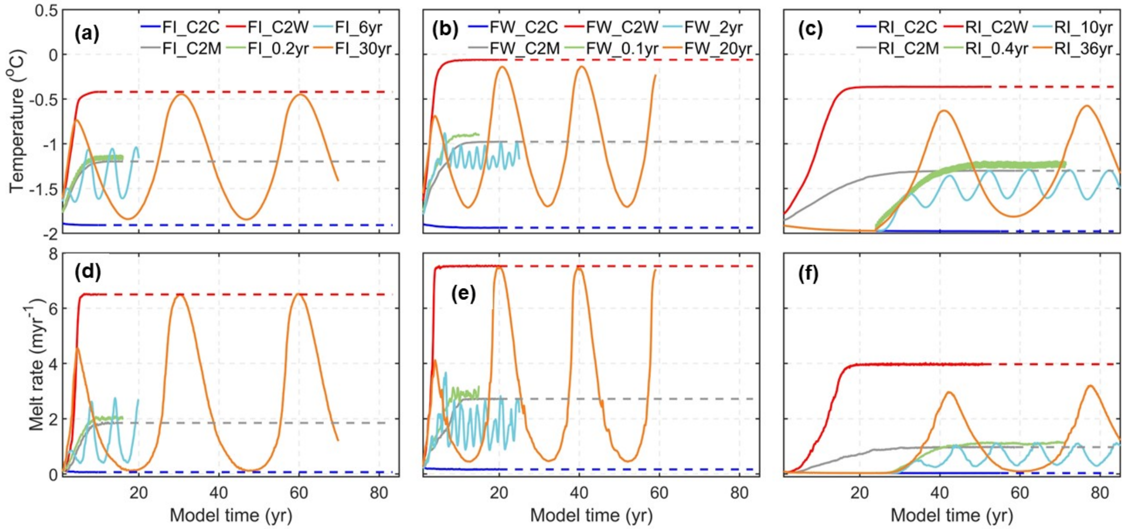

Figure 4. ~~Time~~ Panels (a) and (d) show time series of domain-averaged temperatures and cavity-averaged melt rates, respectively, from the selected FVCOM-ISOMIP+ simulations~~in configurations~~. These includes three constant forcing simulations: COLD (~~a~~FI_C2C)~~FVCOM-ISOMIP+~~, MEAN (~~b~~FI_C2M)~~FVCOM-Wedge~~, and WARM (~~c~~FI_C2W)~~ROMS-ISOMIP+~~, as well as three oscillating forcing simulations with periods of 0.2 (FI_0.2yr), 6 (FI_6yr), and 30 years (FI_30yr). ~~Time~~ Panels (b) and (e) display time series of domain-averaged temperatures and cavity-averaged melt rates, respectively, from the selected FVCOM-Wedge simulations~~in~~. These includes three constant forcing simulations: COLD (~~d~~FW_C2C)~~FVCOM-ISOMIP+~~, MEAN (~~e~~FW_C2M)~~FVCOM-Wedge~~, and WARM (FW_C2W), as well as three oscillating forcing simulations with periods of 0.1 (FW_0.1yr), 2 (FW_2yr), and 20 years (FW_20yr). Panels (c) and (f) show time series of domain-averaged temperatures and cavity-averaged melt rates, respectively, from the selected ROMS-ISOMIP+ simulations. These includes three constant forcing simulations: COLD (RI_C2C), MEAN (RI_C2M), and WARM (RI_C2W), as well as three oscillating forcing simulations with periods of 0.4 (RI_0.4yr), 10 (RI_10yr), and 36 years (RI_36yr). The dashed lines extend from their respective quasi-steady state values for interpretative purposes.

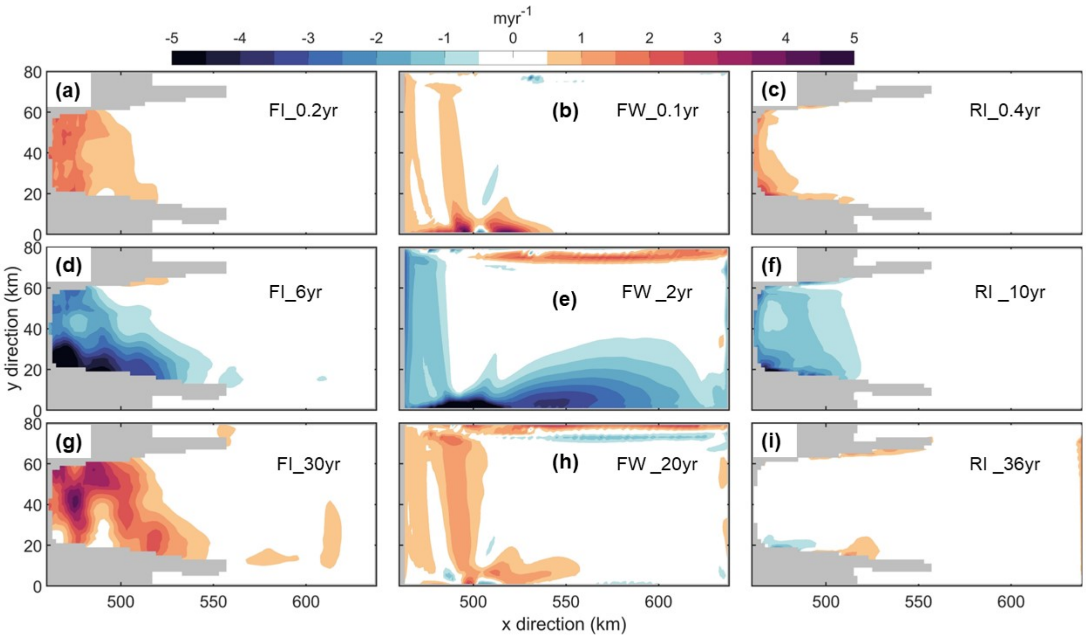

Figure 5. ~~Spatial~~ Panels (a), (d), and (g) show spatial distributions of melt rate deviations from ~~selected~~ the FVCOM-ISOMIP+ oscillating forcing simulations with periods of 0.2 (FI_0.2yr), 6 (FI_6yr), and 30 years (FI_30yr), respectively, relative to ~~their respective~~ the mean-state melt rates~~, across the three model configurations: FVCOM-ISOMIP+~~. Panels (~~a~~b), ~~d,~~(e), and (h) display spatial distributions of melt rate deviations from the FVCOM-Wedge oscillating forcing simulations with periods of 0.1 (~~b~~FW_0.1yr), ~~e,h~~2 (FW_2yr), and ~~ROMS-ISOMIP+~~ 20 years (FW_20yr), respectively, relative to the mean-state melt rates. Panels (c), (f~~,i~~)~~. The top~~, ~~middle,~~ and ~~bottom rows correspond to~~ (i) show spatial distributions of melt rate deviations from the ROMS-ISOMIP+ oscillating forcing simulations with ~~forcing~~ periods ~~significantly shorter~~of 0.4 (RI_0.4yr), ~~approximately equal to~~10 (RI_10yr), and ~~substantially longer than their respective MCRTs~~36 years (RI_36yr), respectively, relative to the mean-state melt rates.

entering the cavity at a temperature close to that of the MEAN profiles, thereby leading to a melting response ~~close to that from~~ that is nearly equivalent to that observed under the MEAN forcing~~simulation~~. Consequently, ~~in this regime, the melting~~ this response exhibits low sensitivity to rapidly varying ocean forcing. ~~Given our earlier assertion that the accelerated forcing approach only remains valid when basal melting response is not sensitive to corresponding accelerations in ocean boundary forcing, we deduce the approach is applicable in this regime. Secondly, all three model configurations show that~~ In contrast, when the oscillating forcing periods greatly exceed the MCRTs, melt rates increase significantly. Specifically, the normalized melt rates ~~drop to~~ increase from about 0.7 ~~for oscillation periods near the MCRTs~~ when the forcing period near the MCRT (Log2(Normalized timescale) ~~$\approx$~~ $\approx$ 0) ~~, marking the lowest normalized melt rates among all oscillating simulations . This suggests that any alteration in the forcing timescale, for instance, changing from~~ to more than 1.1 when the period is much longer than the MCRT (Log2(Normalized timescale) ~~$\approx$ 0 to $\approx$ 2, could significantly impact the melting response. Thus, when~~ $\geq$ 2) for both ISOMIP+ domain configurations. In the FVCOM-ISOMIP+ configuration, the ~~oscillation period of ocean forcing,~~

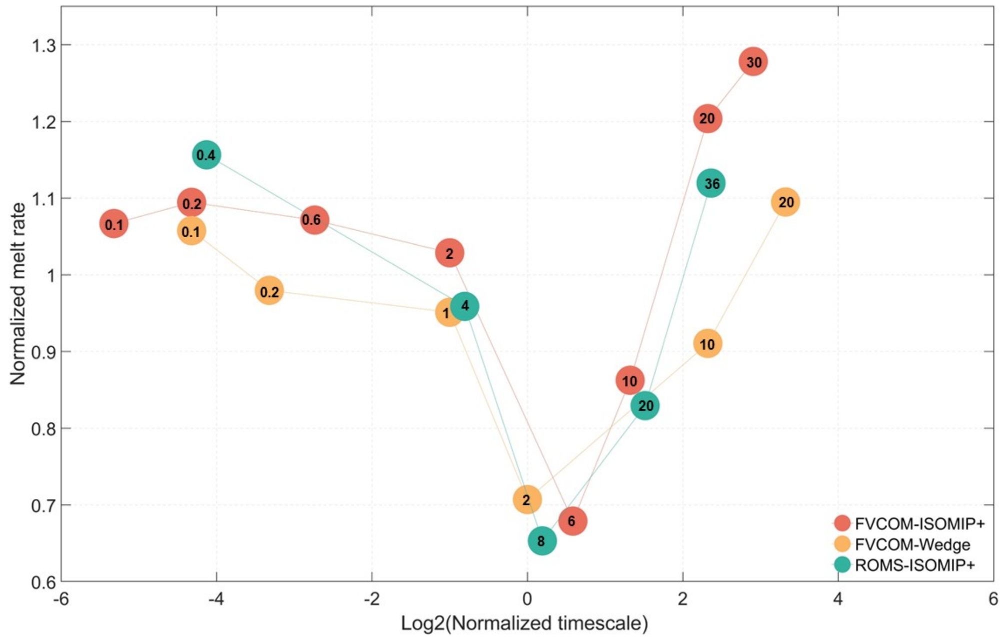

Figure 6. Normalized melt rates plotted against normalized timescales from all the simulations across ~~three~~ the FVCOM-ISOMIP+, FVCOM-Wedge, and ROMS-ISOMIP+ model configurations. The period of oscillating profiles used in each simulation is denoted by the black text within the colored circles.

~~whether under regular or accelerated forcing approaches, approximates the mean cavity residence time, the accelerated forcing~~ normalized melt rate increases to about 1.3 when the forcing period (30 years) is seven times longer than the MCRT of 4 years. In addition, the FVCOM-Wedge simulations display a comparable increasing trend but at a slower rate, likely due to differences in cavity geometry. The increase in melt rates is attributed to the quadratic relationship between melt rates and ocean temperatures (Holland et al., 2008a; Jenkins et al., 2018). In detail, as the ocean forcing oscillates slowly, ocean temperatures tend to follow the oscillatory forcing at every stage. When averaged over the oscillation period, the mean melt rate aligns more closely with that from the WARM forcing and thus is higher than that from the MEAN forcing. We expect that the melting response will stabilize when ocean temperatures fully adjust to the oscillatory forcing. However, due to the lack of simulations with longer periods, we are unable to determine the minimum period necessary for the melting response to stabilize.

In summary, the accelerated forcing approach is likely appropriate in scenarios when the forcing period is either significantly shorter than the MCRT or long enough to allow the melting response to fully adjust to the ocean forcing. In these cases, changes in the forcing timescale lead to a similar mean melting response. However, our approach may not be suitable ~~.~~

when the forcing period, whether accelerated or not, is such that any changes in the forcing timescale likely lead to deviations from the mean melting response. In the following section, we will use coupled ice sheet-ocean experiments to verify these findings and evaluate the accelerated forcing approach.

Table 5. Summary of coupled ice sheet-ocean experiments. For the Constant class, "Rest" in the simulation name indicates the simulation is initialized from the COLD ~~rest state~~rest-state cavity, while "Spunup" indicates the simulation is initialized from the quasi-steady state of the respective regular forcing simulation (acceleration factor 1). The optional suffix "_R" in the simulation name denotes the use of ROMS in the coupled model. The period shown in brackets refers to model time not represented time (which is always 0.6 yr for fast and 30 yr for slow periodic forcing).

Experiment class	Simulation name	Acceleration factor	Restoring forcing profiles (period)
Constant	CRest1(_R)	1	WARM
	CRest3(_R)	3	WARM
	CRest10(_R)	10	WARM
	CSpunup3(_R)	3	WARM
	CSpunup10(_R)	10	WARM
Periodic-fast	PFast1	1	oscillating (0.6 yr)
	PFast3	3	oscillating (0.2 yr)
	PFast10	10	oscillating (0.06 yr)
Periodic-slow	PSlow1	1	oscillating (30 yr)
	PSlow1.5	1.5	oscillating (20 yr)
	PSlow3	3	oscillating (10 yr)

4 Coupled ice sheet-ocean experiments

4.1 Experiment design

To explore the approach's applicability across various ocean models, we conduct our main experiments using two coupled model setups: Elmer/Ice-FVCOM and Elmer/Ice-ROMS.

Our coupled experiments are based on the MISOMIP1 IceOcean1 experiment framework (Asay-Davis et al., 2016). ~~Accordingly, the~~ The ocean model domain is identical to the domain used in the stand-alone ocean experiments (Figure 2), while the ice sheet model domain extends from 0 to 640 km in the x direction. We have structured the coupled experiments into three classes characterized by the timescale of far-field ocean conditions: Constant, Periodic-fast, and Periodic-slow. Each class includes one benchmark simulation under regular forcing and several simulations under accelerated forcing, as listed in Table 5 and explained in detail below.

The Constant class represents a scenario where an ice shelf cavity experiences a regime shift from a cold to a warm cavity. Each coupled model setup has one regular forcing and four accelerated forcing simulations. The regular forcing simulation, identical to the COLD-to-WARM MISOMIP1 IceOcean1r experiment (Asay-Davis et al., 2016), is initialized from the COLD

~~rest state~~ rest-state cavity and restored to the WARM profiles. Two accelerated forcing simulations, using acceleration factors of 3 and 10, are initialized from the COLD ~~rest state~~rest-state cavity. Another two accelerated forcing simulations, with the same acceleration factors, are initialized from the spun-up state of the respective regular forcing simulation. ~~Specifically~~In detail, the FVCOM-based ~~spun-up state is after 144 months simulation in model time and the~~ and ROMS-based ~~spun-up state is after 240 months simulationin model time~~simulations are initialized from the model state at 12 years and 20 years, respectively, of the corresponding regular forcing simulation. All accelerated forcing simulations are restored to the same WARM profiles as the regular forcing simulation. This is because the timescale of a constant forcing can be considered infinite, and any accelerations of it are also infinite. We run simulations for 1200 months in represented time. Note that we use both Elmer/Ice-FVCOM and Elmer/Ice-ROMS for this class. However, due to resource constraints, we only use Elmer/Ice-FVCOM for the following two classes.

The Periodic-fast class represents a scenario where an ice shelf cavity experiences fast-varying far-field ocean conditions with a timescale much shorter than its cavity residence time. The regular forcing simulation is restored to the oscillating profiles with a period of 0.6 years, which is significantly shorter than a MCRT of 4 years. Two accelerated forcing simulations, using acceleration factors of 3 and 10, are restored to the oscillating profiles with periods of 0.2 and 0.06 years in model time, respectively. All simulations in this class are initialized from the ~~240-month spun-up state~~ model state at 12 years of the stand-alone simulation with the MEAN profiles (FI_C2M). We run all simulations for ~~400 months~~ 30 years in represented time, beyond their spin-up phase and reaching a quasi-equilibrium state.

The Periodic-slow class represents a scenario where an ice shelf cavity experiences slow-varying far-field ocean conditions that vary over a timescale significantly longer than its cavity residence time. The regular forcing simulation is restored to the 30-year period oscillating profiles, more than seven times longer than a MCRT of 4 years. Longer periods are not feasible in the current configuration due to computational constraints. Two accelerated forcing simulations, using acceleration factors of 1.5 and 3, are restored to the oscillating profiles with periods of 20 and 10 years in model time, respectively. All simulations in this class are initialized from the ~~600-month~~ 50-year spun-up state of the stand-alone ~~simulation forced with the 30-year oscillating profiles (FI_30yr)~~FVCOM-ISOMIP+ oscillating forcing simulation with a period of 30 years. We run all simulations for ~~690 months~~ 55 years in represented time.

4.2 Evaluating the accelerated forcing approach

We now evaluate the accelerated forcing approach by directly comparing key diagnostics relevant to basal melting from the ~~corresponding~~ accelerated forcing simulations to those from the ~~corresponding~~ regular forcing simulation within each of the three experiment classes. These diagnostics include time series of cavity-averaged melt rates and ocean volume changes, along with spatial distributions of melt rates~~. We also assess spatial distributions of~~ , and integrated ice draft changes ~~and grounding line positions~~ at the end of the simulation. Note that the spatial distributions of melt rates are time-averaged over over the last year of represented time for the Constant class, the last 6 years of represented time for the Periodic-fast class, and over the last cycle of represented time for the Periodic-slow class. Additionally, given that the absolute differences in ocean-driven melting under the accelerated forcing are concentrated near the grounding line across all experiment classes—a detail that will be elaborated on below—and considering that marine ice sheets are sensitive to melt patterns near the grounding line, we also evaluate grounding line positions throughout the simulation to assess the net effect of melting differences on ice dynamics under accelerated forcing.

4.2.1 Constant far-field ocean conditions

~~In the CRest simulations where the ocean model starts~~ When the coupled model is initialized from the COLD ~~rest state~~ rest-state cavity and undergoes the WARM forcing, the FVCOM-based ~~coupled system takes a similar period (110 months in model time~~ simulations take a similar time (about 11 years) to adjust to the transient forcing changes, whether under regular forcing or accelerated forcing (Figure 7a). During this adjustment, warmer water from the boundaries flushes into the ice cavity, causing melt rates to rise from ~~0–~2.4 $\mathrm{m\,yr^{-1}}$ for all experiments~~ 0 to $\sim 2.4\ \mathrm{m\,yr^{-1}}$ in all simulations, despite the different accelerated ice draft change rates. This pattern indicates that the spin-up duration is mainly dictated by ocean boundary conditions, not by the feedback in the coupled model system. Consequently, the melting response during the spin-up phase in the regular forcing simulation ~~(CRest1)~~ is not reproduced in the accelerated forcing simulations when viewed in represented time (CRest3, CRest10; Figure 7b), suggesting the accelerated forcing approach is not ~~effective~~ applicable during this phase. This conclusion is supported by results from the ROMS-based ~~setup (CRest3_R, CRest10_R to CRest1_R in Figure ??~~simulations (Figure 7b,d).

In contrast, the accelerated forcing simulations initialized from a spun-up state exhibit similar temporal melting response to the regular forcing simulation. For the FVCOM-based setup, both ~~of the two accelerated simulations (CSpunup3, CSpunup10)~~ accelerated forcing simulations yield a constant melt rate of about $2.4\ \mathrm{m\,yr^{-1}}$, nearly identical to that in the regular forcing simulation (~~CRest1~~CSpunup3, CSpunup10; Figure 7b). For the ROMS-based setup, the accelerated forcing approach can effectively capture oscillations in the melt rates, which are primarily attributed to an ocean response to the ice draft changes (Zhao et al., 2022), with comparable frequency and magnitude to those under the regular forcing (Figure 7d). Thus, our subsequent analysis focuses only on the accelerated forcing simulations initialized from ~~a~~ the spun-up ~~ocean~~ state.

~~Furthermore, the spatial pattern of basal melting from the~~ Basal melting in the FVCOM-based accelerated forcing simulations ~~closely matches that from~~ exhibit similar spatial pattern as the regular forcing simulation~~for the FVCOM-based setup~~, with minor exceptions in the deeper parts of the cavity. ~~The spatial pattern in~~ In the regular forcing simulation (~~CRest1)shows enhanced melting~~ Figure 8a), enhanced melting is observed in the deep ice region near the grounding line (x< 450 km) with a region-averaged melt rate of ~~24 $\mathrm{m\,yr^{-1}}$, as shown in Figure 8a~~24 $\mathrm{m\,yr^{-1}}$. Absolute differences in melt rates from both accelerated forcing simulations ~~(CSpunup3, CSpunup10)~~ relative to the regular forcing simulation are lower than ~~0.5 $\mathrm{m\,yr^{-1}}$~~ 0.5 $\mathrm{m\,yr^{-1}}$ across most of the cavity, indicated by the large uncolored areas away from the deep ice region in Figure ~~8c and Figure 8~~8c and e. In the deep ice region, ~~the region-averaged~~ averaged melt rate differences relative to the regular forcing simulation are ~~1.5 $\mathrm{m\,yr^{-1}}$ and 3 $\mathrm{m\,yr^{-1}}$ for the accelerated forcing simulations with~~ 1.5 $\mathrm{m\,yr^{-1}}$ and 3 $\mathrm{m\,yr^{-1}}$ for the simulations with acceleration factors of 3 and 10, respectively, ~~both representing relative melting changes below 4%~~ corresponding to changes of approximately 6% and 12%.

A similar conclusion can be drawn from the outcome of the ROMS-based coupled simulations, particularly for the lower acceleration factor, as shown in the right column of Figure 8. In specific, visible differences in melt rates from both accelerated forcing simulations (CSpunup3_R,CSpunup10_R) relative to the regular forcing simulation (CRest_R) mainly occur in the newly ungrounded high-melting region (x < 440 km; Figure 8f,hd,f). In this region, the accelerated forcing simulation of with a factor of 3 shows an absolute difference in area-averaged region-averaged melt rate of 5 $\mathrm{m\,yr^{-1}}$, representing a relative change of 6% of the area-averaged region-averaged melt rate of 79 $\mathrm{m\,yr^{-1}}$ seen from the regular forcing simulation (Figure ??d8b). However, this difference increases to the absolute difference is 43 $\mathrm{m\,yr^{-1}}$ in the simulation with an acceleration factor of 10, amounting to a relative change in region-averaged melting beyond 50%. This substantial difference is likely a result of increased draft change rates interacting with the sudden alteration in ice draft slope and corresponding circulation (Zhao et al., 2022).

Time series of ocean volume changes from , likely resulting from a phase shift in the melt rate oscillation (Figure 7d).

Figure 9 displays spatial distributions of integrated ice draft changes and differences between accelerated and regular forcing simulations for both FVCOM-based accelerated forcing simulations (CSpunup3, CSpunup10) also exhibit a remarkable agreement with those from the regular forcing simulation, showing a steady increase from 0 to approximately $2\times10^{12}\mathrm{m}^3$ over the represented 1200 months (as depicted in the black lines in Figure 9a). This reflects continuous mass transfer from ice to ocean under the constant WARM forcing. The ROMS-based simulations shows a similar trend, with discrepancies between the regular and the accelerated forcing remaining below 2% in the last 900 represented months (Figure 9b). Note that the peaks in the accelerated simulation curves are likely attributed to the ROMS-based system's adjustment to the accelerated ice draft change rates, with a higher factor leading to a more pronounced peak.

Additionally, the grounding line positions are consistent between the regular and the accelerated forcing simulations, located at x = 436 km and x = 431 km for the FVCOM-based and the ROMS-based setups, respectively. Deviations in integrated draft changes from the regular forcing simulation under the accelerated forcing are generally small, except near the grounding line. In For the FVCOM-based setup, the integrated ice draft changes in the regular forcing simulation increase from about 50 m at the ice front to approximately 350 m near the original grounding line ($x \approx 460\mathrm{km}$), and then decreases to below 50 m in the newly-ungrounded area (Figure 9ea). The absolute differences in ice draft changes are typically below 5 m for an acceleration factor under the accelerated forcing with a factor of 3 and below 10 m for a factor of 10 across most of the cavity (Figure 9e ,g c and e). However, at certain locations near the grounding line, these differences increases to over 10 m and 20 m for factors of 3 and 10, respectively, representing relative changes exceeding 20% and 40%. In For the ROMS-based setup, integrated ice draft changes in the regular forcing simulation increase from about 50 m at the ice front to over 400 m at approximately 15 km from the grounding line, and then decrease to about 100 m at the grounding line (Figure 9db). While most of the cavity exhibits small deviations similar in magnitude to the FVCOM-based counterparts, significant deviations from the ROMS-based regular forcing simulation in the ROMS-based setup are concentrated within 15 km to the grounding line (Figure 9f,h d and f). At certain locations here, the absolute differences at certain locations exceed 20 m and 50 m for under accelerated forcing with factors of 3 and 10, respectively, corresponding to relative changes of more than 20% and 50%.

While there are significant deviations, exceeding 20% compared to Ice draft changes lead to ocean volume changes in the coupled system. Time series of ocean volume changes from both FVCOM-based and ROMS-based accelerated forcing simulations are almost indistinguishable from those of the corresponding regular forcing simulations, showing a steady increase from 0 to approximately $2\times10^{12}\ \mathrm{m}^3$ and $1.7\times10^{12}\ \mathrm{m}^3$, respectively, over the represented 100 years (Figure 10a and b). Furthermore, time series of grounding line positions along the central line (y = 40 km) show identical grounding line retreat under regular and accelerated forcing with different factors for the FVCOM-based setup (Figure 10c), with only minor variations in the timing of ungrounding of individual model grid elements. Similar conclusion can be drawn from the ROMS-based simulation, except in the ~~regular forcing simulation, in integrated ice draft changes at certain locations in the newly grounded region, our findings~~case of the accelerated forcing simulation with a factor of 10, likely due to the phase shift in melt rate oscillations.

Our findings, as described above, suggest that the accelerated forcing approach is applicable in scenarios where an ice shelf cavity experiences steady far-field ocean conditions. This is particularly true for the lower acceleration factor, evidenced by the less than 10% relative changes in integrated ice draft changes across most of the cavity, less than ~~2% in total ocean volume changes, and less than~~ 6% in melt rates, ~~while maintaining the grounding line positions when using~~ and nearly identical ocean volume changes and grounding line retreat in the case of an acceleration factor of 3 in both FVCOM-based and ROMS-based setups. However, given that the temporal melting response in the accelerated forcing simulations diverges from the regular forcing simulation during the spin-up phase, the accelerated forcing approach is only ~~suited~~ applicable for the spun-up phase.

4.2.2 Fast-varying far-field ocean conditions

~~In~~ When the coupled model ~~exposed~~ is restored to fast-varying ocean conditions with timescale much shorter than the MCRT, the regular forcing simulation ~~(PFast1)~~ shows high-frequency variability in temporal melting response, as depicted by the gray lines in Figure ~~10~~11a. This variability is not captured in the accelerated forcing simulations (~~PFast3/10;~~ red and orange lines in Figure ~~10~~11a). However, for the evolution of the coupled ice-ocean system, the time-averaged is more important than the high-frequency variability. ~~Across all three simulations, we see similar trends in cavity-averaged melt rates.~~ The accelerated forcing simulations exhibit melt rates that fluctuate around the low-pass filtered melt rate time series of the regular forcing simulation (black lines; Figure ~~10~~12a). The maximum deviation in melt rates from the accelerated forcing simulations observed is approximately $0.1\ \mathrm{myr}^{-1}$, less than 10 % of the corresponding melt rate in the regular forcing simulation. This finding agrees well with the results of the stand-alone ocean experiments presented earlier in Section 3, where we illustrate that the mean melting response to fast-varying oscillation ocean forcing converges to the mean-state melting~~response. Likewise, after a spin-up phase of 150 months in represented time, the relative differences in total ocean volume changes between the accelerated and regular forcing simulations remain below 3%, as illustrated in Figure 10b.~~.

The spatial pattern of melting in the regular forcing simulation ~~(PFast1)~~ is characterized by enhanced melting near the grounding line, reaching up to $30\ \mathrm{myr}^{-1}$ (Figure ~~10c)and~~ 12a), with an asymmetric pattern of melting at the lower part and freezing at the upper part of the cavity approximately 20 km away from the grounding line. This ~~spatial pattern shows general assemblance as the pattern seen~~ pattern shows a general similarity to the one observed in the stand-alone MEAN forcing simulation (FI_C2M, Figure 3b). Absolute differences in melt rates from both accelerated forcing simulations ~~(PFast3/10)~~ relative to the regular forcing simulation are lower than $0.5\ \mathrm{myr}^{-1}$ across most of the cavity, indicated by the large uncolored

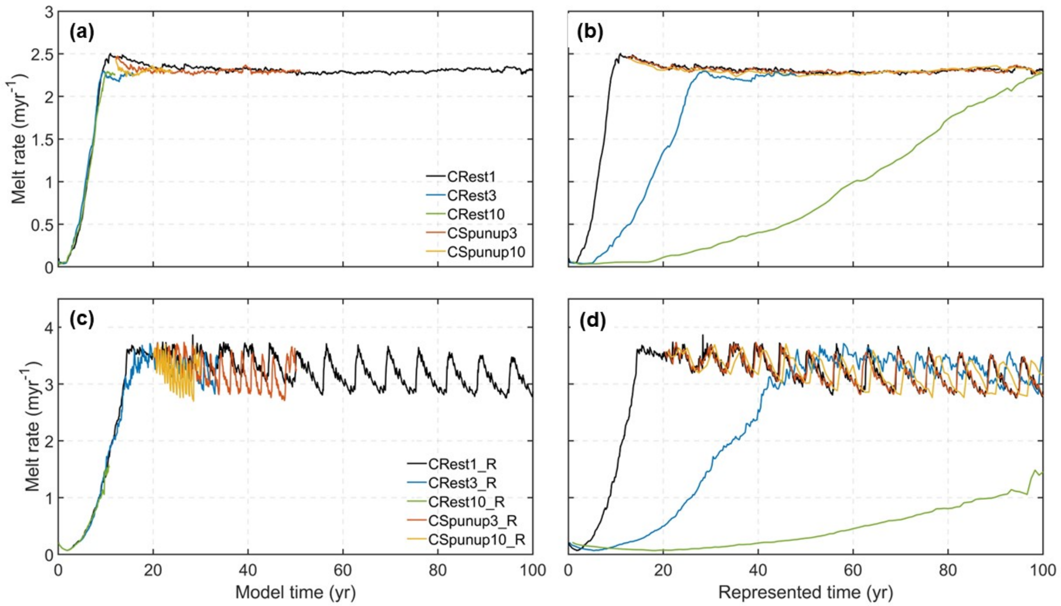

Figure 7. Time Panels (a) and (b) show time series of cavity-averaged melt rates derived from the FVCOM-based coupled simulations in terms of (a) model time and (b) represented time, respectively. Time The simulations include the regular forcing simulation (CRest1), the accelerated forcing simulations initialized from the COLD rest-state cavity with factors of 3 (CRest3) and 10 (CRest10), and the accelerated forcing simulations initialized from the spun-up state with factors of 3 (CSpunup3) and 10 (CSpunup10). Panels (c) and (d) show time series of cavity-averaged melt rates derived from the ROMS-based coupled simulations in terms of (c) model time and (d) represented time, respectively. These simulations include the regular forcing simulation (CRest1_R), the accelerated forcing simulations initialized from the COLD rest-state cavity with factors of 3 (CRest3_R) and 10 (CRest10_R), and the accelerated forcing simulations initialized from the spun-up state with factors of 3 (CSpunup3_R) and 10 (CSpunup10_R).

areas away from the grounding line in Figure 10e and 10g12c and e. However, notable deviations in melt rates compared to the regular forcing simulation are observed near the grounding line when using a higher acceleration factor of 10. Here exists under the accelerated forcing with a factor of 10 (Figure 12e). In this region, there are a few locations of melt rate differences exceeding 15 myr^{-1}, more than half of that from the which is more than 50 % of the corresponding melt rate in the regular forcing simulation (Figure 10g).

As a result of the melting pattern, the most pronounced reductions in integrated draft reductions in the regular forcing simulation are observed at the lower flank of the cavity and near the grounding line, reaching up to 200 m (Figure 10d12b). Absolute deviations in integrated draft changes from the accelerated forcing simulation with a factor of 3 (PFast 3) relative to the regular forcing simulation are small, generally below 2 m across most of the cavity, with a few points near the grounding line exceeding 5 m (Figure 1012d). In the accelerated forcing simulation with a higher factor of 10(PFast 10), the absolute deviations increase are larger, especially in the inner part of the cavity (x <500 km), with a few locations exceeding 20 m near

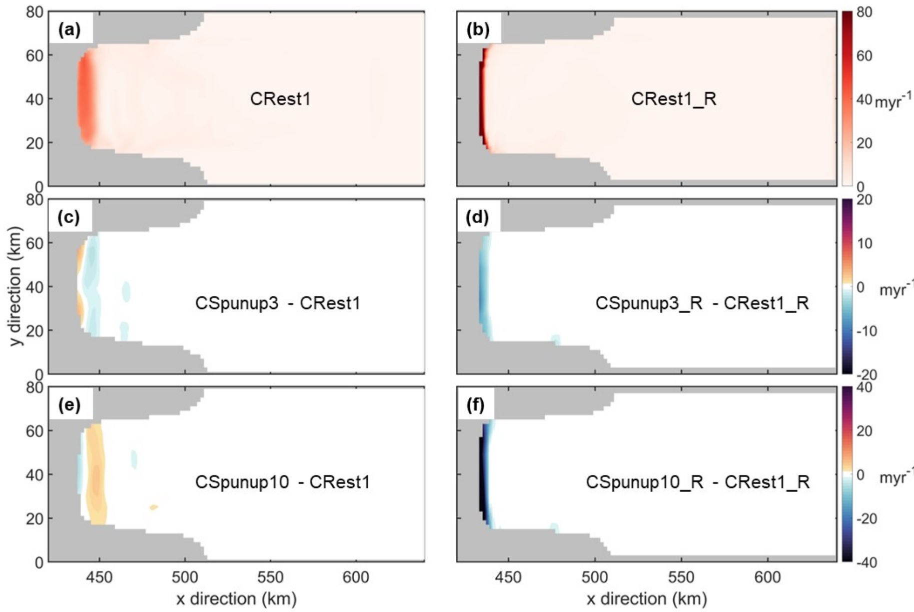

Figure 8. ~~Panel~~ Panels (a) ~~shows spatial distributions of~~ and (b) show melt rates from the FVCOM-based regular forcing simulation ~~,~~ (CRest1) and ~~panels~~ the ROMS-based regular forcing simulation (~~e~~CRest1_R), respetively. Panels (c) and (e) ~~show spatial distributions of difference~~ display the differences in melt rates from ~~both~~ the FVCOM-based accelerated forcing simulations with factors of 3 (CSpunup3) and 10 (CSpunup10), respectively, relative to the regular forcing simulation. ~~Panel~~ Panels (~~b~~d) ~~shows spatial distributions of melt rates from the ROMS-based regular forcing simulation,~~ and ~~panels~~ (~~d,~~ f) ~~shows spatial distributions of difference~~ show the differences in melt rates from ~~both~~ the ROMS-based accelerated forcing simulations with factors of 3 (CSpunup3_R) and 10 (CSpunup10_R), respectively, relative to the regular forcing simulation.

the grounding line (Figure 10~~h). The~~ f). Time series of the total volume changes (Figure 11b) and the grounding line positions ~~are consistent across the three simulations at x = 435 km~~(Figure 11c) are nearly identical over the 30 years of represented time under the regular and accelerated forcing.

In summary, ~~except the relative differences in melt rates~~our analyses indicate that the accelerated forcing simulations generally reproduce the temporal melting response, spatial distributions of melt rates, and integrated ice draft changes~~exceed~~. Relative changes in these variables are kept under 10% across most locations. However, at a few ~~locations in the vicinity of the grounding linewhen we use~~ points near the grounding line, relative differences in melt rates and integrated ice draft changes exceed 10% when a higher acceleration factor of 10 ~~, the accelerated forcing simulations can reproduce the time-averaged melting response,~~ is used. Despite these discrepancies, the total ocean volume changes ~~, spatial distributions of melt rates and integrated ice draft changes, with a relative change of less than 10%. Thus~~and the grounding line retreat remain identical under accelerated forcing compared to those under regular forcing. Therefore, we consider the accelerated forcing approach ~~to be~~

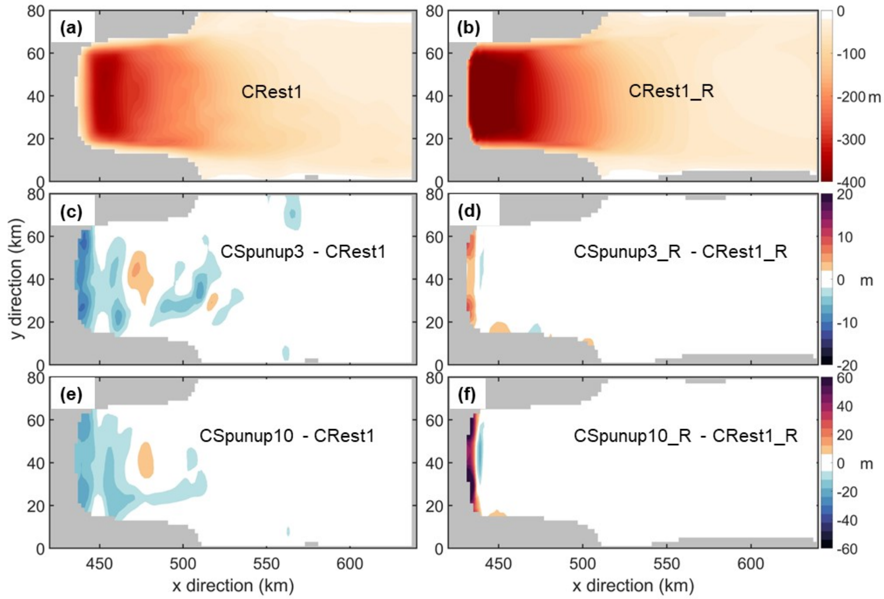

Figure 9. ~~Time series of ocean volume changes from the regular forcing simulation~~ Panels (~~depicted by black lines) along with absolute differences in percentages in ocean volume changes from both accelerated forcing simulations relative to the regular forcing simultion, derived from (~~a) ~~the FVCOM-based setup~~ and (b) ~~the ROMS-based setup (b). Panel (c) shows spatial distributions of~~ show integrated ice draft changes from the FVCOM-based regular forcing simulation (CRest1) and the ROMS-based regular forcing simulation (CRest1_R), respectively. Panels (c) and ~~panels~~ (e~~, g~~) ~~show spatial distributions of difference~~ display the differences in integrated draft changes from ~~both~~ the FVCOM-based accelerated forcing simulations with factors of 3 (CSpunup3) and 10 (CSpunup10), respectively, relative to the regular forcing simulation. ~~Panel~~ Panels (d) ~~shows spatial distributions of integrated ice draft changes from the ROMS-based regular forcing simulation,~~ and ~~panels~~ (f~~, h~~) show ~~spatial distributions of difference~~ the differences in integrated draft changes from ~~both~~ the ROMS-based accelerated forcing simulations with factors of 3 (CSpunup3_R) and 10 (CSpunup10_R), respectively, relative to the regular forcing simulation.

suitable when the forcing timescale is significantly shorter than the mean cavity residence time, as ~~suggested~~ supported by our findings from the stand-alone ocean experiments.

4.2.3 Slow-varying far-field ocean conditions

~~In~~ When the coupled model ~~forced with~~ is subjected to slow-varying ~~oscillation~~ ocean conditions with a timescale much longer than ~~its CMRT~~the MCRT, the regular forcing simulation ~~(PSlow1) displays~~ exhibits a temporal melting response with an oscillation pattern ~~of~~ matching the period of the ocean forcing, approximately a 30-year period in represented time, as depicted by the black lines in Figure ~~11a. This pattern reflects the period of ocean forcing in the regular forcing simulation. In the~~ 14a. Although both accelerated forcing simulations ~~, although~~ capture the oscillation period~~is captured~~, there is a noticeable

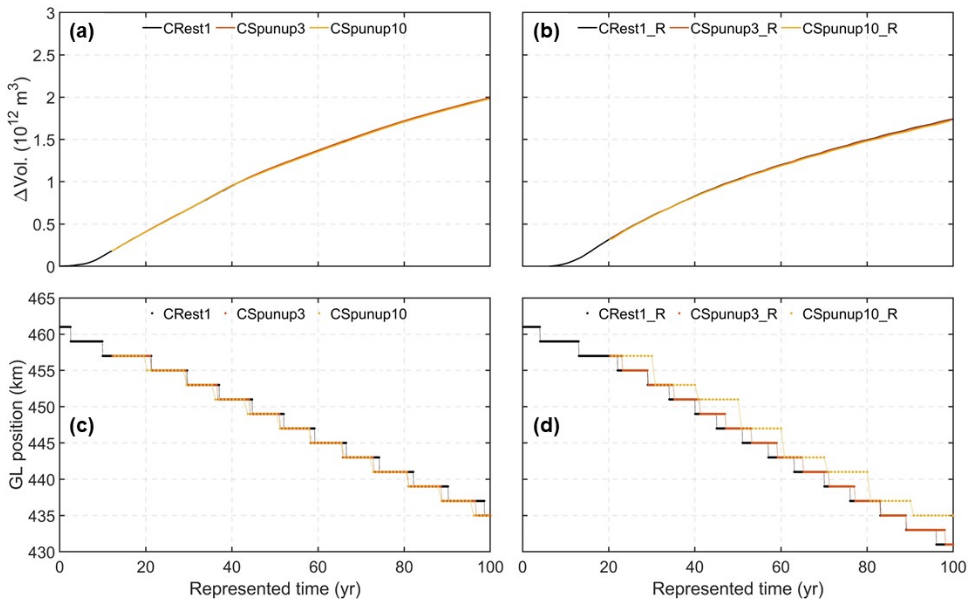

Figure 10. Panels (a) and (c) show time series of total ocean volume changes and grounding line (GL) positions, respectively, from the FVCOM-based regular forcing simulation (CRest1) and the accelerated forcing simulations with factors of 3 (CSpunup3) and 10 (CSpunup10). Panels (b) and (d) display time series of total ocean volume changes and GL positions, respectively, from the ROMS-based regular forcing simulation (CRest1_R) and the accelerated forcing simulations with factors of 3 (CSpunup3_R) and 10 (CSpunup10_R).

reduction in oscillation amplitude, shown by the red and orange lines in Figure ~~11~~14a. Specifically, in the second cycle, peak melt rates decrease from approximately $5\ \mathrm{myr}^{-1}$ ~~in PSlow1~~ under the regular forcing to about $4\ \mathrm{myr}^{-1}$ ~~in the simulation with an acceleration~~ under the accelerated forcing with a factor of 1.5~~(PSlow1.5), and further~~, and to approximately $2\ \mathrm{myr}^{-1}$ with a factor of ~~3 (PSlow3).~~ 3. This reduction in melting amplitude agrees well with findings from our stand-along experiments presented in Section 3, which indicate that melting decreases when the ocean forcing period is not significantly different from the MCRT. In ~~PSlow3, the 10-year~~ the accelerated forcing simulation with a factor of 3, the ocean forcing period is ~~not significantly different from the~~ adjusted from 30 years under the regular forcing to 10 years, which is closer to the MCRT of 4 years, ~~in contrast to the 30-year period in PSlow1,~~ resulting in significantly reduced melting. In addition, the asymmetrical melt rate curve in ~~PSlow1, which is~~ the regular forcing simulation, characterized by a rapidly rising peak, slower decline, and a prolonged period of low melt ~~and relates to internal feedbacks of~~ — due to internal feedback between the cavity circulation ~~with the forcing~~ , and forcing — becomes less pronounced ~~in PSlow1.5 and almost disappears in PSlow3, as illustrated in Figure 11a . This indicates that the equilibrium response when the forcing period is significantly longer than the CMRT, can not be fully developed in the case of accelerated ocean conditions. Furthermore, Figure 11b reveals significant differences in total ocean volume changes across the three simulations. By the end of the simulation, the total changes amount to $0.62 \times 10^{12}\mathrm{m}^3$, $0.4 \times 10^{12}\mathrm{m}^3$, and $0.18 \times 10^{12}\mathrm{m}^3$ in PSlow1, PSlow1.5, and PSlow3, respectively. This represents relative differences of~~

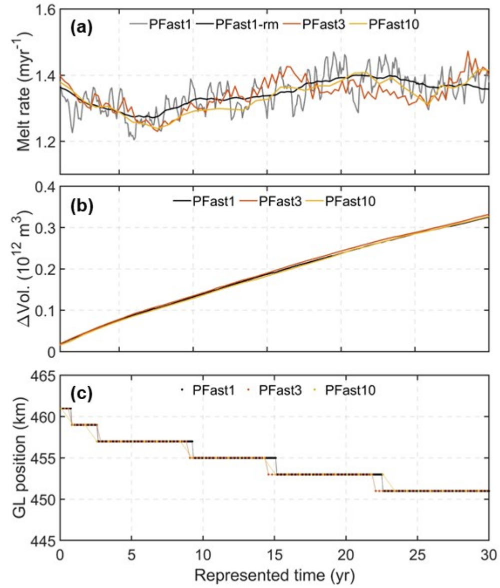

Figure 11. Time series of (a) cavity-averaged melt ratesacross all simulations in the Periodic-fast class, and (b) ocean volume changes, and (c) grounding line (GL) positions from the regular forcing simulation (depicted by black linesPFast1) along with absolute differences in ocean volume changes from both and the accelerated forcing simulations relative to the regular forcing simulation. Panel with factors of 3 (ePFast3) shows spatial distributions of melt rates from the regular forcing simulation, and panels 10 (e, gPFast10)show spatial distributions of difference in melt rates from both accelerated forcing simulations relative to the regular forcing simulation. Panel Also shown in (da) shows spatial distributions is a low-pass filtered version of integrated ice draft changes the melt rate time series from the regular forcing simulation , and panels (f, hPFast1-rm)show spatial distributions of difference in ice draft changes from both accelerated forcing simulations relative to the regular forcing simulation.

approximately 35% and 70% in the two accelerated forcing simulations. with an acceleration factor of 1.5 and nearly disappears with a factor of 3.

The spatial melting pattern in PSlow 1.5 and PSlow3 also notably differs patterns of melting in both accelerated forcing simulations notably differ from that in PSlow1. Specifically, Pslow1 the regular forcing simulation. In detail, basal melting under the regular forcing exhibits a spatial pattern similar to that observed in the stand-alone MEAN ocean forcing simulation (FI_C2M, Figure 3b), manifested as a high-melting zone exceeding 50 myr^{-1} near the grounding lineand , with an asymmetric pattern of melting and freezing 20 km away from the grounding line , as shown in Figure 11c(Figure 14a). However, this high-melting zone is less evident in PSlow1.5 and PSlow3 under the accelerated forcing with factors of 1.5 (Figure 14c) and 3 (Figure 11e,g14e). This discrepancy extends to is also reflected in integrated ice draft changes: significant reductions of more than in ice draft, exceeding 300 m near the grounding line in PSlow1 under the regular forcing (Figure 11 d)14b), are only

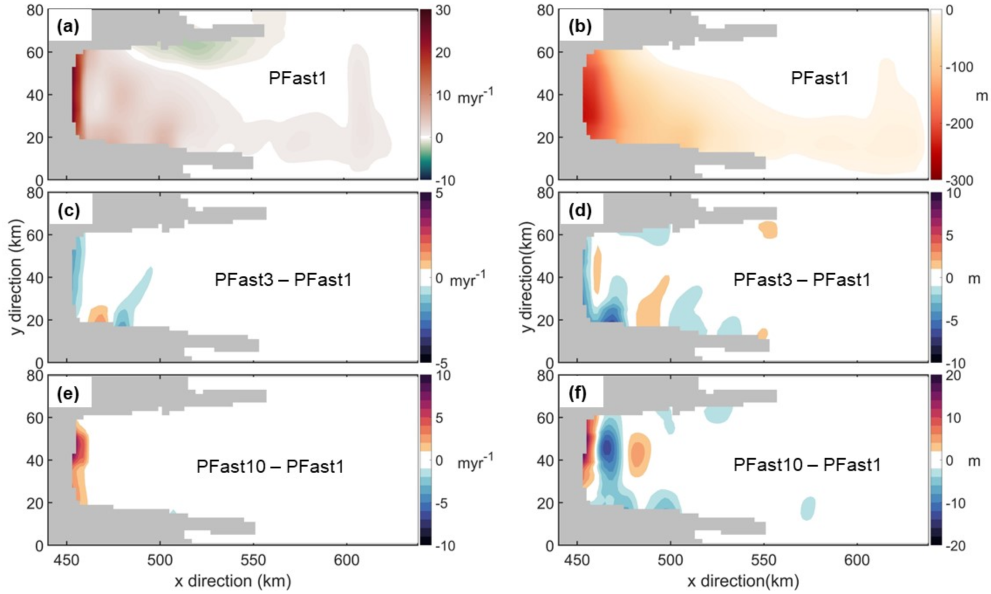

Figure 12. Panel (a) shows spatial distributions of melt rates from the regular forcing simulation (PFast1), while panels (c, e) display the differences in melt rates from the accelerated forcing simulations with factors of 3 (PFast3) and 10 (PFast10) relative to the regular forcing simulation. Panel (b) shows the spatial distribution of integrated ice draft changes from the regular forcing simulation (PFast1), with panels (d) and (f) showing the differences in ice draft changes from the accelerated forcing simulations with factors of 3 (PFast3) and 10 (PFast10) relative to the regular forcing simulation.

partially visible ~~PSlow1.5~~ with an accelerated factor being 1.5 (Figure ~~11 f~~14d) and nearly absent ~~in PSlow3~~ with a factor of 3 (Figure ~~11 h). The grounding line also retreats less in PSlow3 and PSlow1.5 than in PSlow1, with positions~~ 14f).

Figure 13b displays time series of total ocean volume changes across the three simulations. It reveals significant differences between the regular and accelerated forcing simulations. By the end of the simulation, the total changes amount to $0.62 \times 10^{12}\mathrm{m}^3$, $0.4 \times 10^{12}\mathrm{m}^3$, and $0.18 \times 10^{12}\mathrm{m}^3$ under the regular forcing and the accelerated forcing with factors of 1.5 and 3, respectively. This corresponds to relative differences of approximately 35% and 70% in the accelerated forcing simulations with factors of 1.5 and 3, respectively. The time series of grounding line positions (Figure 13b) also shows notable differences between the regular and accelerated forcing simulations, with the grounding line retreating less under the accelerated forcing. By the end of the simulation, the grounding line positions are at $x =$ ~~455~~ 445 km, 451 km, and ~~445 km~~ 455 km under the regular forcing and the accelerated forcing with factors of 1.5 and 3, respectively.

In summary, the accelerated forcing simulations, particularly ~~PSlow3~~with the factor of 3, do not effectively replicate the melting response observed in the regular forcing simulation~~(PSlow1)~~. This is largely attributable to the ~~accelerated~~ adjusted timescale of ocean forcing in ~~PSlow3~~ the accelerated simulation being close to the mean cavity residence time.

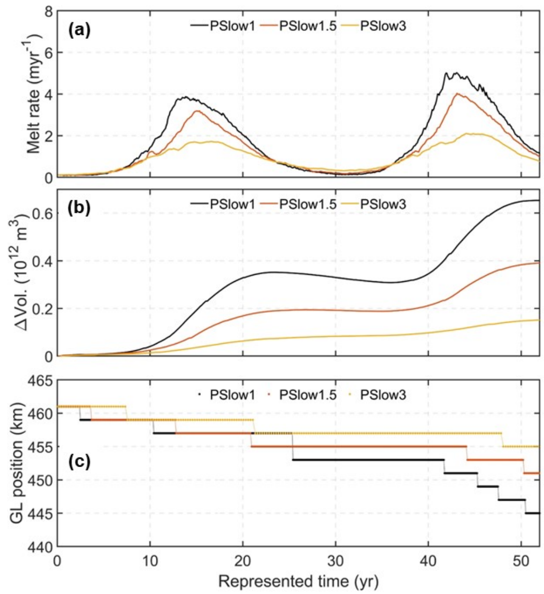

Figure 13. Time series of (a) cavity-averaged melt rates~~and~~ , (b) ocean volume changes~~across all simulations in~~ , and (c) grounding line (GL) positions from the ~~Period-slow class~~regular forcing simulation (PSlow1) and the accelerated forcing simulations with factors of 1.5 (PSlow1.5) and 3 (PSlow3). The first ~~34 months~~ 3 years are considered ~~model~~ the spin-up phase and are excluded from the analysis. ~~Panels (c, e, g) show spatial distributions of melt rates, and panels (d, f, h) show spatial distributions of integrated ice draft changes derived from all simulations.~~

5 Discussion and conclusions

In this study, we have introduced the accelerated forcing approach to address the discrepancy in timescales between the ice sheet and ocean ~~models~~ components in coupled modelling. This approach, which extends the ocean simulation duration by a constant acceleration factor, has been evaluated within the MISOMIP1 framework across three scenarios representing varied far-field ocean conditions categorized ~~based on their relation~~ by the relative magnitude of the forcing timescale to the mean cavity residence time.

The mean cavity residence time, ~~an intrinsic timescale of the ocean model and~~ mainly determined by the cavity geometry ~~, can be quantified by the stand-alone ocean experiments~~and barotropic transport, is an intrinsic timescale of an ice shelf cavity. It represents the ~~period~~ time needed for the cavity to ~~adjust to a~~ reach an equilibrium melting state, where the cavity is filled with water that is exactly in balance with the steady ocean boundary forcing (Holland, 2017). When the timescale of ~~unsteady~~ the varying ocean forcing approaches this intrinsic timescale, ~~there will be interactions~~ interactions occur between basal melting, cavity circulation, ~~the~~ heat inertia within the cavity, and transient changes in ~~the boundary forcing~~boundary forcing, leading to a melting minimum. Consequently, the melting response becomes highly sensitive to any alterations in these factors. This scenario ~~challenges~~ tests the underlying assumption of the accelerated forcing approach ~~:~~ that basal melting response is not

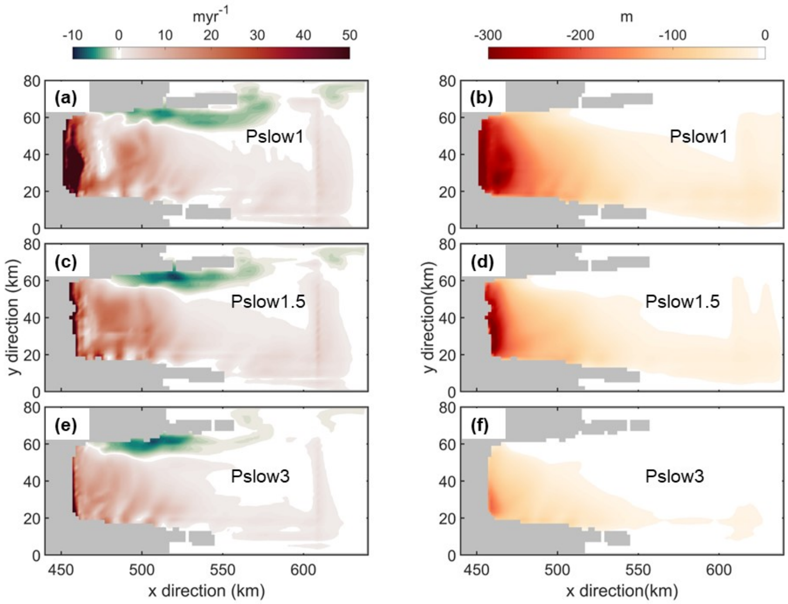

Figure 14. Panels (a, c, e) show spatial distributions of melt rates, while panels (b, d, f) depict spatial distributions of integrated ice draft changes. These results are derived from the regular forcing simulation (PSlow1) and the accelerated forcing simulations with factors of 1.5 (PSlow1.5) and 3 (PSlow3), respectively.

sensitive to corresponding accelerations in ocean boundary forcing. ~~Therefore~~Hence, the accelerated forcing approach ~~loses effectiveness~~ likely loses applicability when the forcing timescale, whether under regular or accelerated forcing~~approaches, is in the order of the mean~~ , is close to the mean cavity residence time. This limitation should be considered when applying our approach to real-world scenarios. For example, the El Niño-Southern Oscillation (ENSO), which significantly influences regions like the Amundsen Sea (Paolo et al., 2018; Huguenin et al., 2024), may be poorly represented under accelerated forcing due to its typical 2-7 year cycle coinciding with the cavity residence time of certain ice shelves around Antarctica. Notably, cold-water shelves with large areal extent, such as the Fichner-Ronne Ice Shelf and the Ross Ice Shelf have a cavity residence time of 4-8 years (Nicholls and Østerhus, 2004; Loose et al., 2009). This alignment could lead to an overestimation of the melting response when ENSO's timescale is compressed under accelerated forcing. Moreover, even if the multi-decadal variation in forcing substantially exceeds the cavity residence time, applying the accelerated forcing approach may result in an underestimation of basal melting response once its compressed timescale is comparable to the cavity residence time. Therefore, caution should be used when applying the accelerated forcing approach to studies addressing climate variability on sub-decadal to decadal timescales.

However, when the ocean forcing varies over a timescale much shorter than the cavity residence time, the ocean model system behaves similarly to a low-pass filter. In this case, the time-average melting response is less coupled with the varying boundary forcing and tends to converge to a stable state produced by the time-averaged forcing, making it insensitive to changes in timescales of the forcing, as observed in the Fast-varying experiment class. This scenario upholds the assumption of the accelerated approach. Therefore, ~~in the Fast-varying experiment class, the~~ the accelerated forcing approach ~~effectively reproduces the melting response seen with regular forcing~~ can be applicable when the ocean forcing varies on seasonal timescale.

When the timescale of the ocean forcing significantly exceeds the cavity residence time, the ~~model system has enough time to respond to each forcing phase, allowing the melting to stabilize at an equilibrium state at all phases~~ cavity is flushed several times during each cycle. Unlike with steady ocean forcing, the cavity can never fully achieve the equilibrium melting state under oscillating ocean forcing (Holland, 2017). Nevertheless, if the period is sufficiently long, waters at each phase of the forcing cycle ~~. This process is well elucidated in (Holland, 2017). The same pattern is evident in the melt rate time series from the stand-alone FVCOM-ISOMIP simulation with a 30-year oscillating forcing, where the forcing timescale significantly exceeds the mean cavity residence time of 4 years. We anticipate that for forcings with timescales exceeding~~ may have enough time to be flushed into the cavity, allowing the melting to reach a quasi-equilibrium state. This state closely approximates equilibrium but includes slight fluctuations due to the continuous variation in forcing. For instance, a period of 30 ~~years, melting would also reach equilibrium in each phase, with a consistent~~ years seems long enough for the FVCOM-ISOMIP+ configuration to this quasi-equilibrium melting state at each phase of the cycle. Figure 4d illustrates that the minimum mean melt rate in FI_30yr deviates slightly from that under the COLD forcing, indicating that even the coldest waters have enough time to fill the cavity and influence melting. This suggests that warmer water phases, especially the warmest, are also sufficiently flushed into the cavity to reach a quasi-equilibrium melting state, as evidenced by the maximum mean melt rate ~~averaged over the respective cycles. Consider a case in which the forcing timescale is 300 years,~~ being nearly the same as that under the WARM forcing. Considering a hypothetical 300-year forcing period, waters in each phase of the cycle would have 10 times ~~the~~ longer to influence the cavity compared to the 30-year ~~period, the melting will reach a similar equilibrium state at every phase of the 300-year cycle, but over a phase period~~ cycle, allowing the quasi-equilibrium melting state in each phase to last about 10 times longer. Therefore, the melting response in any single phase of the 300-year cycle can be ~~reflected~~ approximated by the response in the corresponding single phase of the 30-year cycle~~. This upholds the fundamental assumption~~ , supporting the fundamental assumptions of the accelerated forcing approach. ~~While we haven't~~ Note that we have not tested forcings with ~~oscillation~~ periods longer than 30 years due to resource constraints. However, the constant forcing in the Constant experiment class essentially represents an infinitely slow varying force once the model reaches a ~~quasi-equilibrium state. Consequently, the~~ quasi-steady state. This highlights the potential applicability of the accelerated forcing approach ~~successfully replicated the melting response observed under regular forcing~~ in ~~this experiment class, except for ice draft changes and melt rates near the grounding line, which warrant further investigation.~~ century-long cavity-processes-oriented modelling studies, which could improve the accuracy of projections of Antarctica's contribution to sea level rise. In such projections, the slowly varying background forcing would not be periodic but instead steadily increasing at comparably slow rates in global warming scenarios. However, the linearly increasing trend from cold to warm can be considered as a warming phase of varying forcing over even longer timescales far exceeding the mean cavity residence time of any ice shelf, ensuring the applicability of the accelerated forcing approach.

~~Our~~ For scenarios involving mixed timescales, such as seasonal forcing superimposed on decadal oscillations with a steady background increase, additional experiments are necessary to yield definitive answers. Addressing these complex interactions requires a broader range of studies to fully understand the dynamics at play. These studies would help clarify how various overlapping timescales influence each other, which is essential for more accurate climate modeling. Such investigations, however, fall beyond the scope of our current study and represent important directions for future research.

Neverthless, our study demonstrates that the accelerated forcing approach can ~~be a useful tool in coupled ice sheet-ocean modelling. The approach can~~ directly contribute to the MISOMIP1 project by reducing the required simulation time of 100 years, depending on the acceleration factors. Applying the accelerated approach with a factor of 3 for the IceOcean1 experiment has reduced the spun-up simulation duration by a factor of 3 and reproduced most of the melting diagnostics within 10% of those with the regular forcing approach across two participating coupled models. Recommending the accelerated forcing approach to other participating models within the ~~MISOMIP1~~ MISOMIP framework would provide a more comprehensive understanding of the robustness and applicability of the approach in idealized model setups.

~~Moreover, there is no reason to believe that the~~ Furthermore, our current evaluation of the approach has been conducted using the IceOcean1 setup, where the calving front is fixed. It would be worthwhile to explore the applicability of the accelerated forcing approach ~~is inapplicable to real-world scenarios. This approach could be applicable in modelling studies related to Antarctica's contribution to sea level rise projections, particularly when the ocean forcing varies over century-long timescales. These timescales vastly exceed the mean cavity residence time of any single iceshelve around Antarctica . For instance, cold-water ice shelves like the Fichner-Ronne Ice shelf and the Ross Ice Shelf have a cavityresidence time of approximately 4-8 years (Nicholls and Østerhus, 2004; Loose et al., 2009). Warmer-water ice shelves like those in the Amundsen Sea have even shorter cavity residence times, given their smaller sizes and faster melting-driven cavity circulations. In such cases,~~ using the IceOcean2 setup, which is similar to the ~~timescales in the accelerated ocean forcingtimescales, when applying the approach, would still be significantly longer than the shelves' residence time of a few years, ensuring the effectiveness of the accelerated~~ IceOcean1 setup but includes dynamic calving. This extension could enhance our understanding of the ocean's response to calving fluxes under accelerated forcing, which will be discussed in detail in the following paragraph.

It is important to acknowledge the limitations of our idealized study. When investigating the sensitivity of melting responses to changes in the timescale of the boundary conditions, we have only considered the lateral ocean conditions and changes in the ice draft, assuming these factors predominantly control the cavity circulation and, thus, the basal melting. This simplification presents challenges when applied to real-world scenarios where other boundary conditions affecting the cavity properties, as well as the open ocean, can not be ignored. One of them is the total glacial meltwater input to the ocean, comprising melt due to iceberg calving, basal melting, and subglacial discharge (from the subglacial hydrologic system). Numerous studies have highlighted the significant impact of glacial meltwater on ocean stratification, with important consequences for the evolution of sea ice(Bintanja et al., 2013; Merino et al., 2018; Goldberg et al., 2023), Antarctic bottom water formation (Li et al., 2023), ocean currents around Antarctica (Nakayama et al., 2021; Gwyther et al., 2023; Moorman et al., 2020), (Bronselaer et al., 2018; Purich anc
. The current study, which focuses on fine-resolution ice sheet-ocean interactions at the Antarctic margins, specifically the ice shelf cavity, includes only the ocean-driven melt component of glacial meltwater. This is because basal meltwater has the

largest impact on cavity circulation, mainly through buoyancy forcing. Larger-scale studies would also need to quantify the impact of other components of glacial meltwater, especially the calving flux, under accelerated forcing.

Furthermore, adjustments in glacial meltwater input are necessary to realistically represent its impacts on ocean and climate under the accelerated forcingapproach. . Without such adjustments, the total freshwater flux into the Southern Ocean would not be consistent with that under the regular forcing, potentially distorting climate simulations. However, accelerating the meltwater flux introduces its own challenges. A significant increase in local freshwater input over a short period can drastically alter local salinity gradients and stratification. This disruption can affect everything from mixing processes to ocean currents, potentially leading to unrealistic model behavior. Following Lofverstrom et al. (2020), we propose not accelerating the meltwater flux in order to maintain realistic local ocean dynamics. Instead, to mitigate the inconsistent freshwater input in the accelerated simulations, we suggest applying periodic restoration techniques to adjust the ocean's salinity and temperature fields using observed or targeted values (Griffies et al., 2009, 2016; Lofverstrom et al., 2020). Moreover, we expect similar inconsistencies in atmospheric boundary conditions—such as precipitation (freshwater input), and wind and radiation fluxes (energy input)-under the accelerated forcing. The aforementioned periodic restoration techniques can also help reduce the effects of these inconsistencies, thereby ensuring more representative freshwater and energy inputs in the ocean model.

Testing across various acceleration factors in the three coupled experiment classes has also revealed a trade-off between computational efficiency and integrity in melting response. While higher acceleration factors reduce simulation duration more, they also introduce larger deviations in melting response. This necessitates a careful balance between computational efficiency and the integrity of the modeled melting response.

While we have used a fixed cavity residence time in interpreting our experiment results, the cavity residence time in coupled models varies due to cavity geometry and circulation changes. This poses a challenge when using the accelerated forcing approach: the basal melting integrity maintained for a specific acceleration factor might not hold for another. Time-varying acceleration factors could address the challenge and require exploration in future developments.

Last, we emphasize that applying the accelerated forcing approach and choosing the acceleration factor should be evaluated case-by-case, with careful judgment and sensitivity testing.

Code availability. The coupled model used the ice sheet model Elmer/Ice Version 9.0 (https://github.com/ElmerCSC/elmerfem.git;Gagliardini et al. (2013)), the ocean model FVCOM (https://github.com/UK-FVCOM-Usergroup/uk-fvcom/tree/akvaplan_dev, Zhou and Hattermann (2020)), the ocean model ROMSIceShelf Version:1.0 with code (https://doi.org/10.5281/zenodo.3526801; Galton-Fenzi (2009)), and the coupled framework FISOC Version 1.1 (https://doi.org/10.5281/zenodo.4507182; Gladstone et al. (2021)). The FISOC-ROMSIceShelf-Elmer/Ice source code and input files needed to run the ROMS-based coupled experiments in this study are all publicly available (https://doi.org/10.5281/zenodo.5908713, Zhao et al. (2022)). The FISOC-FVCOM-Elmer/Ice model shares the same ice sheet model input files as the FISOC-ROMS-Elmer/Ice model. The FVCOM-based coupled simulations use the same ice sheet model input files as the ROMS-based coupled simulations. The ocean model input files and model results for the FVCOM-based simulations are all publicly preserved at the Norwegian national research data archive and can be downloaded anonymously by anyone via a web-based interface (https://doi.org/10.11582/2024.00122).

Author contributions. QZ, RG, and TH conceptualized and designed the study, CZ and BGZ contributed to the experiment design. QZ implemented the experiments using FVCOM, and CZ implemented the experiments using ROMS and Elmer/Ice. QZ led the analysis and wrote the initial draft. All authors contributed to the discussion of the results and paper writing.

Competing interests. The authors declare that they have no conflict of interest.

Acknowledgements. Qin Zhou received financial support from the Norwegian Research Council ~~project 295075. Chen Zhao~~ under projects 295075 and ~~Ben~~ 343397. Chen Zhao was supported by the Australian Research Council Discovery Early Career Researcher Award (DE240100267) and the Australian Government through the Antarctic Science Collaboration Initiative program (ASCI000002). Benjamin Galton-Fenzi ~~received grant~~ also received funding from the ~~Australian Government as part of the~~ Antarctic Science Collaboration Initiative program (ASCI000002). Tore Hattermann ~~acknowledges~~ received financial support from the Norwegian Research Council project 280727. Rupert Gladstone was supported by the Academy of Finland ~~grant numbers~~ grants 322430 and 355572, and by the Finnish Ministry of Education and Culture and CSC - IT Center for Science (Decision diary number OKM/10/524/2022). David Gwyther was supported by the Australian Research Council Discovery Project Grant DP220102525. The authors wish to acknowledge Sigma2 HPC, Norway, and CSC – IT Center for Science, Finland, for providing computational resources.

References

Asay-Davis, X. S., Cornford, S. L., Durand, G., Galton-Fenzi, B. K., Gladstone, R. M., Gudmundsson, G. H., Hattermann, T., Holland, D. M., Holland, D., Holland, P. R., Martin, D. F., Mathiot, P., Pattyn, F., and Seroussi, H.: Experimental design for three interrelated marine ice sheet and ocean model intercomparison projects: MISMIP v. 3 (MISMIPC), ISOMIP v. 2 (ISOMIPC) and MISOMIP v. 1 (MISOMIP1), Geosci. Model Dev., 9, 2471–2497, 2016.

Bintanja, R., van Oldenborgh, G. J., Drijfhout, S., Wouters, B., and Katsman, C.: Important role for ocean warming and increased ice-shelf melt in Antarctic sea-ice expansion, Nature Geoscience, 6, 376–379, 2013.

Bronselaer, B., Winton, M., Griffies, S. M., Hurlin, W. J., Rodgers, K. B., Sergienko, O. V., Stouffer, R. J., and Russell, J. L.: Change in future climate due to Antarctic meltwater, Nature, 564, 53–58, 2018.

Chen, C., Liu, H., and Beardsley, R. C.: An unstructured, finite-volume, three-dimensional, primitive equation ocean model: application to coastal ocean and estuaries., J. Atm. Oceanic Tech., 2003.

Dinniman, M., Klinck, J. M., and Smith, W. O.: Influence of sea ice cover and icebergs on circulation and water mass formation in a numerical circulation model of the Ross Sea, Antarctica, J. Geophys. Res., 112, doi:10.1029/2006JC004036, 2007.

Dutrieux, P., Stewart, C., Jenkins, A., Nicholls, K. W., Corr, H. F., Rignot, E., and Steffen, K.: Basal terraces on melting ice shelves, Geophysical Research Letters, 41, 5506–5513, https://doi.org/10.1002/2014GL060618, 2014.

Edwards, T. L., Nowicki, S., Marzeion, B., Hock, R., Goelzer, H., Seroussi, H., Jourdain, N. C., Slater, D. A., Turner, F. E., Smith, C. J., et al.: Projected land ice contributions to twenty-first-century sea level rise, Nature, 593, 74–82, 2021.

Favier, L., Durand, G., Cornford, S. L., Gudmundsson, G. H., Gagliardini, O., Gillet-Chaulet, F., Zwinger, T., Payne, A., and Le Brocq, A. M.: Retreat of Pine Island Glacier controlled by marine ice-sheet instability, Nature Climate Change, 4, 117–121, 2014.

Favier, L., Jourdain, N. C., Jenkins, A., Merino, N., Durand, G., Gagliardini, O., Gillet-Chaulet, F., and Mathiot, P.: Assessment of sub-shelf melting parameterisations using the ocean–ice-sheet coupled model NEMO(v3.6)–Elmer/Ice(v8.3), Geoscientific Model Development, 12, 2255–2283, https://doi.org/10.5194/gmd-12-2255-2019, 2019.

Foldvik, A., Gammelsrød, T., Østerhus, S., Fahrbach, E., Rohardt, G., Schröder, M., Nicholls, K. W., Padman, L., and Woodgate, R. A.: Ice shelf water overflow and bottom water formation in the southern Weddell Sea, J. Geophys. Res.., 109, C02 015, doi:10.1029/2003JC002008, 2004.

Gagliardini, O., Zwinger, T., Gillet-Chaulet, F., Durand, G., Favier, L., de Fleurian, B., Greve, R., Malinen, M., Martín, C., Råback, P., Ruokolainen, J., Sacchettini, M., Schäfer, M., Seddik, H., and Thies, J.: Capabilities and performance of Elmer/Ice, a new-generation ice sheet model, Geoscientific Model Development, 6, 1299–1318, https://doi.org/10.5194/gmd-6-1299-2013, 2013.

Galton-Fenzi, B.: Modelling Ice-Shelf/Ocean Interaction, Ph.D. thesis, University of Tasmania, 2009.

Galton-Fenzi, B. K., Hunter, J. R., Coleman, R., Marsland, S. J., and Warner, R. C.: Modeling the basal melting and marine ice accretion of the Amery Ice Shelf, J. Geophys. Res., 117, C09 031, https://doi.org/10.1029/2012JC008214, 2012.

Gladstone, R., Payne, A. J., and Cornford, S. L.: Resolution requirements for grounding-line modelling: sensitivity to basal drag and ice-shelf buttressing, Annals Of Glaciology, 53, 97–105, https://doi.org/10.3189/2012AoG60A148, 2012.

Gladstone, R., Galton-Fenzi, B., Gwyther, D., , Q., Hattermann, T., Zhao, C., Jong, L., Xia, Y., Guo, X., Petrakopoulos, K., Zwinger, T., Shapero, D., and Moore, J.: The Framework For Ice Sheet–Ocean Coupling (FISOC) V1.1, GMD, 14, 889–905, https://doi.org/10.5194/gmd-14-889-2021, 2021.

Goldberg, D., Snow, K., Holland, P., Jordan, J., Campin, J.-M., Heimbach, P., Arthern, R., and Jenkins, A.: Representing grounding line migration in synchronous coupling between a marine ice sheet model and a z-coordinate ocean model, Ocean Modelling, 125, 45–60, 2018.

Goldberg, D. N., Twelves, A. G., Holland, P. R., and Wearing, M. G.: The nonlocal impacts of Antarctic subglacial runoff, 2023.

Griffies, S. M., Biastoch, A., Böning, C., Bryan, F., Danabasoglu, G., Chassignet, E. P., England, M. H., Gerdes, R., Haak, H., Hallberg, R. W., et al.: Coordinated ocean-ice reference experiments (COREs), Ocean modelling, 26, 1–46, 2009.

Griffies, S. M., Danabasoglu, G., Durack, P. J., Adcroft, A. J., Balaji, V., Böning, C. W., Chassignet, E. P., Curchitser, E., Deshayes, J., Drange, H., et al.: OMIP contribution to CMIP6: Experimental and diagnostic protocol for the physical component of the Ocean Model Intercomparison Project, Geoscientific Model Development, p. 3231, 2016.

Gwyther, D. E., Dow, C. F., Jendersie, S., Gourmelen, N., and Galton-Fenzi, B. K.: Subglacial freshwater drainage increases simulated basal melt of the Totten Ice Shelf, Geophysical Research Letters, 50, e2023GL103 765, 2023.

Hellmer, H. H., Kauker, F., Timmermann, R., Determann, J., and Rae, J.: Twenty-first-century warming of a large Antarctic ice-shelf cavity by a redirected coastal current, Nature, 485, 225–228, https://doi.org/10.1038/nature11064, 2012.

Holland, D. M., Thomas, R. H., DeYoung, B., Ribergaard, M. H., and Lyberth, B.: Acceleration of Jakobshavn Isbræ triggered by warm subsurface ocean waters., Nat. Geosci., 1, 659–664, doi:10.1038/NGEO316, 2008a.

Holland, P. R.: The Transient Response of Ice Shelf Melting to Ocean Change, Journal of Physical Oceanography, 47, 2101–2114, https://doi.org/10.1175/JPO-D-17-0071.1, 2017.

Holland, P. R., Jenkins, A., and Holland, D. M.: The Response of Ice Shelf Basal Melting to Variations in Ocean Temperature, J. Climate, 21, 2558–2572, https://doi.org/10.1175/2007JCLI1909.1, 2008b.

Huguenin, M. F., Holmes, R. M., Spence, P., and England, M. H.: Subsurface warming of the West Antarctic continental shelf linked to El Niño-Southern Oscillation, Geophysical Research Letters, 51, e2023GL104 518, 2024.

Jenkins, A.: A simple model of the ice shelf–ocean boundary layer and current, Journal of Physical Oceanography, 46, 1785–1803, 2016.

Jenkins, A., Nicholls, K. W., and Corr, H. F. J.: Observation and Parameterization of Ablation at the Base of Ronne Ice Shelf, Antarctica, J. Phys. Oceanogr., 40, 2298–2312, https://doi.org/10.1175/2010JPO4317.1, 2010.

Jenkins, A., Shoosmith, D., Dutrieux, P., Jacobs, S., Kim, T. W., Lee, S. H., Ha, H. K., and Stammerjohn, S.: West Antarctic Ice Sheet retreat in the Amundsen Sea driven by decadal oceanic variability, Nature Geoscience, 11, 733–738, 2018.

Jourdain, N. C., Mathiot, P., Merino, N., Durand, G., Le Sommer, J., Spence, P., Dutrieux, P., and Madec, G.: Ocean circulation and sea-ice thinning induced by melting ice shelves in the Amundsen Sea, J. Geophys. Res., 122, 2550–2573, https://doi.org/10.1002/2016JC012509, 2017.

Jourdain, N. C., Asay-Davis, X., Hattermann, T., Straneo, F., Seroussi, H., Little, C. M., and Nowicki, S.: A protocol for calculating basal melt rates in the ISMIP6 Antarctic ice sheet projections, The Cryosphere, 14, 3111–3134, 2020.

Lesse, G., Roelvink, J. A., van Kester, J., and Stelling, G.: Development and validation of a three-dimensional morphological model, Coastal engineering, 36, 883–915, 2004.

Li, D., DeConto, R. M., Pollard, D., and Hu, Y.: Competing climate feedbacks of ice sheet freshwater discharge in a warming world, Nature Communications, 15, 5178, 2024.

Li, L., Storms, J., and Walstra, D.: On the upscaling of process-based models in deltaic applications, Geomorphology, 304, 201–213, 2018.

Li, Q., England, M. H., Hogg, A. M., Rintoul, S. R., and Morrison, A. K.: Abyssal ocean overturning slowdown and warming driven by Antarctic meltwater, Nature, 615, 841–847, 2023.

Lofverstrom, M., Fyke, J. G., Thayer-Calder, K., Muntjewerf, L., Vizcaino, M., Sacks, W. J., Lipscomb, W. H., Otto-Bliesner, B. L., and Bradley, S. L.: An efficient ice sheet/Earth system model spin-up procedure for CESM2-CISM2: Description, evaluation, and broader applicability, Journal of Advances in Modeling Earth Systems, 12, e2019MS001 984, 2020.

Loose, B., Schlosser, P., Smethie, W. M., and Jacobs, S.: An optimized estimate of glacial melt from the Ross Ice Shelf using noble gases, stable isotopes, and CFC transient tracers, J. Geophys. Res., 114, 15 PP., https://doi.org/200910.1029/2008JC005048, 2009.

McCormack, F., Roberts, J., Gwyther, D., Morlighem, M., Pelle, T., and Galton-Fenzi, B.: The impact of variable ocean temperatures on Totten Glacier stability and discharge, Geophysical Research Letters, 48, e2020GL091 790, 2021.

Merino, N., Jourdain, N. C., Le Sommer, J., Goosse, H., Mathiot, P., and Durand, G.: Impact of increasing antarctic glacial freshwater release on regional sea-ice cover in the Southern Ocean, Ocean Modelling, 121, 76–89, 2018.

Moorman, R., Morrison, A. K., and McC. Hogg, A.: Thermal responses to Antarctic ice shelf melt in an eddy-rich global ocean–sea ice model, Journal of Climate, 33, 6599–6620, 2020.

Morgan, J. A., Kumar, N., Horner-Devine, A. R., Ahrendt, S., Istanbullouglu, E., and Bandaragoda, C.: The use of a morphological acceleration factor in the simulation of large-scale fluvial morphodynamics, Geomorphology, 356, 107 088, 2020.

Muntjewerf, L., Sacks, W. J., Lofverstrom, M., Fyke, J., Lipscomb, W. H., Ernani da Silva, C., Vizcaino, M., Thayer-Calder, K., Lenaerts, J. T., and Sellevold, R.: Description and Demonstration of the Coupled Community Earth System Model v2–Community Ice Sheet Model v2 (CESM2-CISM2), Journal of Advances in Modeling Earth Systems, 13, e2020MS002 356, 2021.

Nakayama, Y., Cai, C., and Seroussi, H.: Impact of subglacial freshwater discharge on Pine Island Ice Shelf, Geophysical research letters, 48, e2021GL093 923, 2021.

Naughten, K. A., Meissner, K. J., Galton-Fenzi, B. K., England, M. H., Timmermann, R., Hellmer, H. H., Hattermann, T., and Debernard, J. B.: Intercomparison of Antarctic ice-shelf, ocean, and sea-ice interactions simulated by MetROMS-iceshelf and FESOM 1.4, Geoscientific Model Development, 11, 1257–1292, 2018.

Naughten, K. A., De Rydt, J., Rosier, S. H., Jenkins, A., Holland, P. R., and Ridley, J. K.: Two-timescale response of a large Antarctic ice shelf to climate change, Nature communications, 12, 1–10, 2021.

Nicholls, K. W. and Østerhus, S.: Interannual variability and ventilation timescales in the ocean cavity beneath Filchner-Ronne Ice Shelf, Antarctica, Journal of Geophysical Research: Oceans, 109, 2004.

Paolo, F., Padman, L., Fricker, H., Adusumilli, S., Howard, S., and Siegfried, M.: Response of Pacific-sector Antarctic ice shelves to the El Niño/Southern oscillation, Nature geoscience, 11, 121–126, 2018.

Pelle, T., Morlighem, M., Nakayama, Y., and Seroussi, H.: Widespread Grounding Line Retreat of Totten Glacier, East Antarctica, Over the 21st Century, Geophysical Research Letters, 48, e2021GL093 213, https://doi.org/https://doi.org/10.1029/2021GL093213, e2021GL093213 2021GL093213, 2021.

Pelletier, C., Fichefet, T., Goosse, H., Haubner, K., Helsen, S., Huot, P.-V., Kittel, C., Klein, F., Le clec'h, S., van Lipzig, N. P. M., Marchi, S., Massonnet, F., Mathiot, P., Moravveji, E., Moreno-Chamarro, E., Ortega, P., Pattyn, F., Souverijns, N., Van Achter, G., Vanden Broucke, S., Vanhulle, A., Verfaillie, D., and Zipf, L.: PARASO, a circum-Antarctic fully coupled ice-sheet–ocean–sea-ice–atmosphere–land model involving f.ETISh1.7, NEMO3.6, LIM3.6, COSMO5.0 and CLM4.5, Geoscientific Model Development, 15, 553–594, https://doi.org/10.5194/gmd-15-553-2022, 2022.

Purich, A. and England, M. H.: Projected impacts of Antarctic meltwater anomalies over the twenty-first century, Journal of Climate, 36, 2703–2719, 2023.

Richter, O., Gwyther, D. E., Galton-Fenzi, B. K., and Naughten, K. A.: The Whole Antarctic Ocean Model (WAOM v1.0): development and evaluation, GMD, 15, 617–647, https://doi.org/10.5194/gmd-15-617-2022, 2022.

Roberts, W. H., Valdes, P. J., and Payne, A. J.: Topography's crucial role in Heinrich Events, Proceedings of the National Academy of Sciences, 111, 16 688–16 693, 2014.

Sausen, R. and Voss, R.: Techniques for asynchronous and periodically synchronous coupling of atmosphere and ocean models: Part 1: general strategy and application to the cyclo-stationary case, Climate Dynamics, 12, 313–323, 1996.

Schoof, C.: Ice-sheet acceleration driven by melt supply variability, Nature, 468, 803–806, https://doi.org/10.1038/nature09618, 2010.

Seroussi, H., Nakayama, Y., Larour, E., Menemenlis, D., Morlighem, M., Rignot, E., and Khazendar, A.: Continued retreat of Thwaites Glacier, West Antarctica, controlled by bed topography and ocean circulation, Geophysical Research Letters, 44, 6191–6199, https://doi.org/https://doi.org/10.1002/2017GL072910, 2017.

Seroussi, H., Nowicki, S., Payne, A. J., Goelzer, H., Lipscomb, W. H., Abe-Ouchi, A., Agosta, C., Albrecht, T., Asay-Davis, X., Barthel, A., Calov, R., Cullather, R., Dumas, C., Galton-Fenzi, B. K., Gladstone, R., Golledge, N. R., Gregory, J. M., Greve, R., Hattermann, T., Hoffman, M. J., Humbert, A., Huybrechts, P., Jourdain, N. C., Kleiner, T., Larour, E., Leguy, G. R., Lowry, D. P., Little, C. M., Morlighem, M., Pattyn, F., Pelle, T., Price, S. F., Quiquet, A., Reese, R., Schlegel, N.-J., Shepherd, A., Simon, E., Smith, R. S., Straneo, F., Sun, S., Trusel, L. D., Van Breedam, J., van de Wal, R. S. W., Winkelmann, R., Zhao, C., Zhang, T., and Zwinger, T.: ISMIP6 Antarctica: a multi-model ensemble of the Antarctic ice sheet evolution over the 21st century, The Cryosphere, 14, 3033–3070, https://doi.org/10.5194/tc-14-3033-2020, 2020.

Seroussi, H., Verjans, V., Nowicki, S., Payne, A. J., Goelzer, H., Lipscomb, W. H., Abe Ouchi, A., Agosta, C., Albrecht, T., Asay-Davis, X., et al.: Insights on the vulnerability of Antarctic glaciers from the ISMIP6 ice sheet model ensemble and associated uncertainty, The Cryosphere Discussions, 2023, 1–28, 2023.

Shchepetkin, A. F. and McWilliams, J. C.: The Regional Ocean Modeling System (ROMS): A split-explicit, free-surface, topography-following coordinates ocean model, Ocean Model., 9, 347–404, 2005.

Siahaan, A., Smith, R. S., Holland, P. R., Jenkins, A., Gregory, J. M., Lee, V., Mathiot, P., Payne, A. J., Ridley, J. K., and Jones, C. G.: The Antarctic contribution to 21st-century sea-level rise predicted by the UK Earth System Model with an interactive ice sheet, The Cryosphere, 16, 4053–4086, 2022.

Smith, R. S., Mathiot, P., Siahaan, A., Lee, V., Cornford, S. L., Gregory, J. M., Payne, A. J., Jenkins, A., Holland, P. R., Ridley, J. K., et al.: Coupling the UK Earth System Model to dynamic models of the Greenland and Antarctic ice sheets, Journal of Advances in Modeling Earth Systems, 13, e2021MS002 520, 2021.

Timmermann, R. and Goeller, S.: Response to Filchner–Ronne Ice Shelf cavity warming in a coupled ocean–ice sheet model – Part 1: The ocean perspective, Ocean Sci., 13, 765–776, https://search.proquest.com/docview/1940938744?accountid=17260, 2017.

Van Achter, G., Fichefet, T., Goosse, H., Pelletier, C., Haubner, K., and Pattyn, F.: Ocean–Ice Sheet Coupling in the Totten Glacier Area, East Antarctica: Analysis of the Feedbacks and Their Response to a Sudden Ocean Warming, Geosciences, 13, 106, 2023.

Voss, R., Sausen, R., and Cubasch, U.: Periodically synchronously coupled integrations with the atmosphere-ocean general circulation model ECHAM3/LSG, Climate Dynamics, 14, 249–266, 1998.

Zhao, C., Gladstone, R., Galton-Fenzi, B. K., Gwyther, D., and Hattermann, T.: Evaluation of an emergent feature of sub-shelf melt oscillations from an idealized coupled ice sheet–ocean model using FISOC (v1.1) – ROMSIceShelf (v1.0) – Elmer/Ice (v9.0), Geoscientific Model Development, 15, 5421–5439, https://doi.org/10.5194/gmd-15-5421-2022, 2022.

Zhou, Q. and Hattermann, T.: Modeling ice shelf cavities in the unstructured-grid, Finite Volume Community Ocean Model: Implementation and effects of resolving small-scale topography, Ocean Modelling, 146, 101 536, https://doi.org/https://doi.org/10.1016/j.ocemod.2019.101536, 2020.